



Evaluation of CALIOP
532 nm AOD over
opaque water clouds

Z. Liu et al.

This discussion paper is/has been under review for the journal Atmospheric Chemistry and Physics (ACP). Please refer to the corresponding final paper in ACP if available.

Evaluation of CALIOP 532 nm AOD over opaque water clouds

Z. Liu^{1,2}, D. Winker², A. Omar², M. Vaughan², J. Kar^{1,2}, C. Trepte², Y. Hu², and G. Schuster²

¹Science Systems and Applications, Inc., Hampton, Virginia, USA

²NASA Langley Research Center, Hampton, Virginia, USA

Received: 11 August 2014 – Accepted: 2 September 2014 – Published: 12 September 2014

Correspondence to: Z. Liu (zhaoyan.liu@nasa.gov)

Published by Copernicus Publications on behalf of the European Geosciences Union.

Title Page

Abstract

Introduction

Conclusions

References

Tables

Figures



Back

Close

Full Screen / Esc

Printer-friendly Version

Interactive Discussion



Abstract

With its height-resolved measurements and near global coverage, the CALIOP lidar onboard the CALIPSO satellite offers a new capability for aerosol retrievals in cloudy skies. Validation of these retrievals is difficult, however, as independent, collocated and co-temporal datasets are generally not available. In this paper, we evaluate CALIOP aerosol products above opaque water clouds by applying multiple retrieval techniques to CALIOP Level 1 profile data and comparing the results. This approach allows us to both characterize the accuracy of the CALIOP above-cloud aerosol optical depth (AOD) and develop an error budget that quantifies the relative contributions of different error sources. We focus on two geographical regions: the African dust transport pathway over the tropical North Atlantic and the African smoke transport pathway over the southeastern Atlantic. Six years of CALIOP observations (2007–2012) from the Northern Hemisphere summer and early fall are analyzed. The analysis is limited to cases where aerosol layers are located above opaque water clouds so that a constrained retrieval technique can be used to directly retrieve 532 nm aerosol optical depth and lidar ratio. For the moderately dense Sahara dust layers detected in the CALIOP data used in this study, the mean/median value of the lidar ratios derived from a constrained opaque water cloud (OWC) technique is $45.1/44.4 \pm 8.8$ sr, which is somewhat larger than the value of 40 ± 20 sr used in the CALIOP level 2 (L2) data products. Comparisons of CALIOP L2 AOD with the OWC-retrieved AOD reveal that for nighttime conditions the L2 AOD in the dust region is underestimated on average by $\sim 26\%$ (0.184 vs. 0.248). Examination of the error sources indicates that errors in the L2 dust AOD are primarily due to use of a lidar ratio which is somewhat too small and to misestimates of dust layer base heights. The mean/median lidar ratio retrieved for smoke is $69.4/70.4 \pm 16.2$ sr, which is consistent with the modeled value of 70 ± 28 sr used in the CALIOP L2 retrieval. Smoke AOD is found to be underestimated, on average, by $\sim 39\%$ (0.191 vs. 0.311). The primary cause of AOD differences in the smoke transport region is the ten-

Evaluation of CALIOP 532 nm AOD over opaque water clouds

Z. Liu et al.

[Title Page](#)[Abstract](#)[Introduction](#)[Conclusions](#)[References](#)[Tables](#)[Figures](#)[Back](#)[Close](#)[Full Screen / Esc](#)[Printer-friendly Version](#)[Interactive Discussion](#)

gency of the CALIOP layer detection scheme to prematurely assign layer base altitudes and thus underestimate the geometric thickness of smoke layers.

1 Introduction

Beginning with the first Intergovernmental Panel on Climate Change (IPCC) assessment, tremendous progress has been made in modeling the global impacts of aerosols on the Earth's climate. But, as summarized in the most recent 5th assessment report (Stocker et al., 2013), significant uncertainties remain. Recent model intercomparisons have shown a large diversity in the vertical distribution of aerosols (Kinne et al., 2006; Textor et al., 2006; Huneus et al., 2011) which can be attributed more to uncertainties in the simulation of aerosol processes than in the realism of the aerosol precursor emissions used by the models. Errors in modeling the vertical distribution of aerosol cause errors in the aerosol atmospheric lifetime and global distribution. In cloudy skies, aerosol radiative forcing can be a strong function of the relative vertical distributions of cloud and aerosol. Comparison with observations is necessary to evaluate and improve model performance, but until recently, global measurements of aerosol vertical distribution were lacking.

The Cloud-Aerosol Lidar with Orthogonal Polarization (CALIOP), deployed aboard the Cloud Aerosol Lidar and Infrared Pathfinder Satellite Observations (CALIPSO) platform, has been acquiring global aerosol and cloud profile data since June 2006 (Winker et al., 2010) and offers a unique opportunity to characterize the global 3-D distribution of aerosol, including aerosol located above low clouds (Winker et al., 2013). Aerosol extinction profiles and aerosol optical depth (AOD) can be derived from the CALIOP measurements even for aerosols located over clouds or other bright surfaces. In contrast, space-based passive sensors have very limited retrieval capabilities in these conditions and thus aerosol retrievals from satellites have been largely limited to aerosol in otherwise clear skies. However, quantifying above-cloud aerosols is required to more accurately assess the aerosol intercontinental transport and radiative and climate impacts

Evaluation of CALIOP 532 nm AOD over opaque water clouds

Z. Liu et al.

Title Page

Abstract

Introduction

Conclusions

References

Tables

Figures



Back

Close

Full Screen / Esc

Printer-friendly Version

Interactive Discussion



(Schulz et al., 2006; Chand et al., 2009; Yu et al., 2012). Very recently Yu et al. (2012) have shown the possibility of above-cloud AOD retrieval that requires synergetic multi-sensor measurements.

CALIOP clear-sky AOD has been evaluated by comparisons with MODIS-Aqua (Kittaka et al., 2011; Redemann et al., 2012) and with AERONET (Schuster et al., 2012; Omar et al., 2013). Several studies have examined seasonal and regional-mean aerosol vertical distributions for the purpose of model evaluation (Yu et al., 2010; Koffi et al., 2012) and noted deficiencies in the vertical aerosol distributions predicted by the models. Validation of the CALIOP retrievals is necessary, of course, but validation of aerosol above clouds is particularly difficult because independent, accurate measurements are almost non-existent. Recently, Winker et al. (2013) reported an initial evaluation of the accuracy of the CALIOP level 3 (gridded, monthly mean) aerosol extinction profiles. These preliminary results showed that monthly-mean CALIOP aerosol profiles provide quantitative characterization of elevated aerosol layers within major transport pathways, but a more detailed validation of the retrievals of these elevated aerosol layers is needed.

In this paper, we refine a previously developed opaque water cloud (OWC) constrained retrieval technique (Hu et al., 2007) and introduce two variations on the standard CALIOP aerosol extinction retrieval algorithm. We then apply these retrievals to nighttime CALIOP 532 nm Level 1 profile data in two regions in the Atlantic Ocean to study the optical properties of transported mineral dust and smoke from biomass fires. Finally, these results are used to evaluate standard CALIOP level 2 (L2) aerosol products.

2 CALIOP data and geophysical regions considered

CALIOP transmits linearly polarized laser light at 532 and 1064 nm. The CALIOP receiver resolves the polarization state of the 532 nm backscatter signals by separately measuring light polarized parallel and perpendicular to the outgoing 532 nm beam.

Evaluation of CALIOP 532 nm AOD over opaque water clouds

Z. Liu et al.

Title Page

Abstract

Introduction

Conclusions

References

Tables

Figures



Back

Close

Full Screen / Esc

Printer-friendly Version

Interactive Discussion



**Evaluation of CALIOP
532 nm AOD over
opaque water clouds**

Z. Liu et al.

Title Page

Abstract

Introduction

Conclusions

References

Tables

Figures



Back

Close

Full Screen / Esc

Printer-friendly Version

Interactive Discussion



Backscatter signals are sampled at a vertical resolution of 30 m below an altitude of 8.2 km and 60 m between 8.2 and 20.2 km. After calibration and range registration, atmospheric layers are detected using a threshold technique applied to profiles of 532 nm attenuated scattering ratio (Vaughan et al., 2009; Winker et al., 2009). Dense clouds can be detected in single-shot profiles, while detection of aerosol layers usually requires averaging of multiple lidar shots. A nested, multi-grid averaging scheme is employed to maximize layer detection probabilities across the broadest possible range of backscatter intensities. To avoid cloud contamination of the aerosol data, boundary layer clouds detected at single shot resolution are identified and removed before further horizontal averaging and subsequent searches for more tenuous layers (Vaughan et al., 2009). After layer detection, a cloud-aerosol discrimination (CAD) algorithm is applied to separate clouds and aerosols (Liu et al., 2009). This CAD process is followed by an algorithm which classifies the aerosol type. Six aerosol types have been defined for the CALIOP retrieval (Dust, Polluted Dust, Marine, Clean Continental, Pollution, and Smoke or Biomass Burning). Each aerosol type is characterized by a mean lidar ratio (i.e., the ratio of aerosol extinction to 180° -backscatter), S_a , that varies from 20–70 sr (Omar et al., 2009). Aerosol extinction is then retrieved at 532 and 1064 nm, using lidar ratios selected according to the aerosol typing results (Young and Vaughan, 2009). Aerosol extinction retrievals are only performed within detected layers, as the CALIOP signal-to-noise ratio (SNR) does not permit retrievals in clear air at the spatial resolution of the L2 products. In this paper, six years (2007–2012) of nighttime CALIOP version 3 (V3) L1 data are analyzed.

The geographic regions considered in this paper are shown by the red boxes in Fig. 1. North Africa is the largest source of dust emissions in the world, injecting large amounts of dust into the atmosphere year round. Transport of Saharan dust across the tropical North Atlantic reaches a maximum during the summer. Cool, moist north-easterly air crossing the Mediterranean into Africa experiences intense heating over the arid continent (e.g., Carlson and Prospero, 1972; Karyampudi et al., 1999). Air over the Sahara is advected westward in the predominantly easterly flow, developing

Evaluation of CALIOP 532 nm AOD over opaque water clouds

Z. Liu et al.

Title Page

Abstract

Introduction

Conclusions

References

Tables

Figures



Back

Close

Full Screen / Esc

Printer-friendly Version

Interactive Discussion



$B'(r) = X(r)/C/\exp(-2S_m \int_{r_0}^r \sigma_m dr')$ is the lidar return signal, normalized (i.e., recalibrated) at r_0 and corrected for molecular attenuation. $X(r)$ is the range-corrected lidar return signal at range r and C is a calibration coefficient determined at the calibration range r_0 . σ_m is the extinction coefficient due to molecular scattering and ozone absorption. β_a and β_m are the aerosol and molecular backscattering coefficients, respectively, with subscripts a and m representing the aerosol and molecular scattering, respectively. $S_a^* = \eta S_a$ where S_a is the aerosol lidar ratio and η is the multiple scattering factor (Platt, 1973). The molecular scattering components can be determined using meteorological data from radiosonde measurements or atmospheric models. In the CALIPSO data processing, a global meteorological analysis product from NASA's Global Modeling and Assimilation Office (GMAO) is used to calculate the necessary molecular backscatter and extinction coefficients. For V3 CALIOP lidar retrievals, the data calibration at 532 nm is performed by comparing return signals from 30–34 km altitudes with a molecular reference profile (Powell et al., 2009).

Iterative numerical solutions have been developed for aerosol retrieval from the lidar return signal (e.g., Elterman, 1966) and have been adopted for the CALIPSO lidar standard data processing (Young and Vaughan, 2009). A form of the iterative numerical solution, accounting for multiple scattering, can be derived from $B'(r)$ by correcting the attenuation due to the particulate scattering (i.e., the exponential term in the following equation) and removing the molecular scattering component $\beta_m(r)$

$$\beta_a(r) = \frac{B'(r)}{\exp\left(-2\eta S_a \int_{r_0}^r \beta_a(r') dr'\right)} - \beta_m(r). \quad (2)$$

The unknown quantity $\beta_a(r)$, is present on both sides of the equation, necessitating an iterative numerical approach to solve Eq. (2).

The lidar ratio S_a is a key parameter in the lidar inversion. S_a is an intrinsic optical property of aerosols that varies depending on the aerosol composition, size distribution, and shape. Once S_a is determined, the aerosol backscatter β_a as well as extinction

$\sigma_a = S_a \times \beta_a$ can be retrieved using either form of the solution. The retrieval accuracy is often dominated by uncertainties in S_a (Young et al., 2013).

3.2 CALIOP standard level 2 retrieval

Three steps are involved in producing the CALIOP standard L2 data products (Winker et al., 2009). First, cloud and aerosol layers are identified by a set of algorithms, referred to as the selective iterative boundary locator (SIBYL) (Vaughan et al., 2009), which are applied to the 532 nm attenuated backscatter profiles. Second, using data from all three CALIOP channels (532 nm parallel and perpendicular channels and 1064 nm channel), layers are identified as clouds or aerosols (Liu et al., 2009) and the aerosol type (Omar et al., 2009) and cloud ice-water phase (Hu et al., 2009) are determined. Finally, profiles of particle backscatter and extinction coefficients are retrieved by the hybrid extinction retrieval algorithm (HERA) (Young and Vaughan, 2009). HERA performs retrievals within the layer boundaries identified by SIBYL using the iterative numerical approach (i.e., Eq. 2) for the backscatter and extinction retrieval. The retrieval is only performed within the layer boundaries identified by SIBYL and the inversion is initiated at the top of the layer. The retrieval requires knowledge of η and layer lidar ratio S_a . In aerosol retrievals, multiple scattering is usually negligible, and hence in V3, $\eta = 1$. S_a is generally selected based on the results of the aerosol typing, though it can be derived directly on those on rare occasions when the air above and below an aerosol layer is free of particles (e.g., as in Young, 1995). Aerosol layers are detected iteratively by SIBYL at horizontal resolutions of 5, 20, and 80 km and the L2 retrieval is performed for all aerosol layers detected at each of these resolutions. Extinction and backscatter profiles are populated in the CALIOP L2 aerosol profile products at a 5 km horizontal resolution. For the layers detected at 20 or 80 km, the retrieved extinction and backscatter coefficients are replicated over 4 or 16 consecutive 5 km profile segments.

Evaluation of CALIOP 532 nm AOD over opaque water clouds

Z. Liu et al.

Title Page

Abstract

Introduction

Conclusions

References

Tables

Figures



Back

Close

Full Screen / Esc

Printer-friendly Version

Interactive Discussion



3.3 Rescaling level 2 AOD

In addition to noise, which is the primary source of random error in the CALIOP measurements and corresponding L2 data products, there are also other sources of error in the derivation of AOD. These include failure to detect the full extent of aerosol layers, due either to SNR-imposed detection limits or algorithm deficiencies, misclassification during aerosol typing, and/or the use of an inaccurate lidar ratio. We cannot simply estimate the AOD error as proportional to the lidar ratio error because the relationship is non-linear (Winker et al., 2009). Instead, to evaluate the impact of lidar ratio errors on AOD due to misclassification of aerosol type, we calculate a rescaled AOD using a procedure similar to that in Lopes et al. (2013).

- a. Integrate the above-cloud aerosol extinction profile to obtain an above-cloud column AOD estimate, τ_{above} , based on the L2 aerosol type and lidar ratio assignments.
- b. Use τ_{above} , the S_a assigned by the CALIOP aerosol subtyping algorithm, and an assumed multiple scattering factor of $\eta = 1$ to derive an estimate of the layer integrated attenuated backscatter via Platt's equation (Platt, 1973):

$$\gamma'_{\text{eff}} = \int_{\text{top}}^{\text{base}} \beta'_a(r) T_a^2(0, r) dr = \frac{1 - \exp(-2\eta\tau_{\text{above}})}{2\eta S_a} \quad (3)$$

where $T_a^2(0, r) = \int_0^z \sigma_a(z) dz$ is the aerosol two-way transmittance between the lidar and the aerosol layer base. For cases where multiple aerosol layers are detected and classified as different aerosol types in the column above an opaque water cloud, Eq. (3) becomes $\gamma'_{\text{eff}} = \sum_{i_{\text{type}}} \frac{1 - \exp(-2\eta\tau_{\text{above}}(i_{\text{type}}))}{2\eta S_a(i_{\text{type}})}$, where i_{type} represents the layer aerosol type, and $S_a(i_{\text{type}})$ and $\tau_{\text{above}}(i_{\text{type}})$ are, respectively, the lidar ratio and the optical depth retrieved for the aerosol of type i_{type} .

23592

Title Page

Abstract

Introduction

Conclusions

References

Tables

Figures



Back

Close

Full Screen / Esc

Printer-friendly Version

Interactive Discussion



- c. Using γ'_{eff} and the lidar ratio for the appropriate aerosol type (dust or smoke), derive an estimate of the rescaled AOD using

$$\text{AOD}_{\text{rescaled}} = -\frac{1}{2\eta S_a} \ln(1 - 2\eta S_a \gamma'_{\text{eff}}) \quad (4)$$

where once again $\eta = 1$ and S_a is either 40 sr (dust) or 70 sr (smoke).

This procedure is applied in the dust and smoke transport regions, assuming that “dust” and “smoke” are the dominant aerosol types in the respective region. While there are always maritime aerosols in the MBL in both regions, for the “aerosol above cloud” cases considered in this paper, boundary layer clouds effectively separate the transported aerosol layers in the free troposphere from the MBL. It is thus highly likely that the above-cloud layers are either dust or smoke, depending on region, and are not mixed with marine aerosol. Further, during the summer months considered in this paper, there is a little chance that cross transport occurs between the two regions, which would presumably produce “polluted dust”. The dust transport and biomass burning activities show a strong seasonal dependence in Africa. In summer, the transport of dust generated in the North Africa occurs primarily over the North Atlantic (D. Liu et al., 2008), while the biomass burning is only active in southern Africa (Haywood et al., 2008). Furthermore, while southern Africa has a large area of arid terrain, it is not a major source of dust production (Washington et al., 2003). A study (based on the first year of the CALIOP measurements (D. Liu et al., 2008) revealed that the occurrence frequency of airborne dust over the southern Africa was small (only few percent for some locations), suggesting that the dust from sources in southern Africa is not readily mobilized by the typical meteorology of the area (Washington et al., 2003). Therefore, the occurrence of dust mixed with smoke (i.e., “polluted dust”) is expected to be small in both regions examined in this study.

Evaluation of CALIOP 532 nm AOD over opaque water clouds

Z. Liu et al.

Title Page

Abstract

Introduction

Conclusions

References

Tables

Figures



Back

Close

Full Screen / Esc

Printer-friendly Version

Interactive Discussion



3.4 Opaque water cloud constrained retrieval

When the layer optical depth is available as a constraint, β_a , σ_a and S_a (or the effective lidar ratio, $S_a^* = \eta S_a$, when multiple scattering effects must be considered) can all be retrieved directly. One well-developed technique to determine the layer optical depth uses the molecular scattering above and below the layer to derive the required constraint (Sassen and Cho, 1992; Young, 1995). When the molecular scattering can be measured in clean air on both sides of a layer, the transmittance (and hence the optical depth) of the layer can be derived by comparing the return signals above and below the layer to a molecular scattering profile derived from rawinsonde measurements or meteorological model data. This technique is applied to the CALIPSO measurements at 532 nm for transparent cirrus clouds in the upper troposphere where the air is generally clean on both above and below the clouds (Young and Vaughan, 2009). Aerosol layers are, however, generally located in the lower troposphere and such clean regions are seldom available.

Recently, Hu et al. (2007) developed a technique for the CALIOP measurements that uses opaque water clouds as a reference to determine the optical depth of overlying transparent aerosol or cirrus layers (e.g., as in Fig. 2). This approach takes advantage of the nearly-constant lidar ratio of water clouds (e.g., Pinnick et al., 1983; O'Connor et al., 2004; Hu et al., 2006), and the well-behaved relationship between the layer-integrated depolarization ratio and the multiple scattering in the layer-integrated attenuated backscatter from water clouds, as described in Hu (2007) by

$$H = \frac{\gamma'_{ss}}{\gamma'_{ms}} = \left(\frac{1 - \delta_l}{1 + \delta_l} \right)^2 \quad (5)$$

where H is the layer effective multiple scattering factor and δ_l is the layer-integrated volume depolarization ratio. The multiple scattering factor that is considered constant in Eqs. (1) and (2) is more rigorously defined in terms of the ratio of single-scattered and multiply-scattered signals from range r , such that $\eta_l(r) = 1 - \ln [B'_{ms}(r)/B'_{ss}(r)] / 2\tau(r)$

Evaluation of CALIOP 532 nm AOD over opaque water clouds

Z. Liu et al.

Title Page

Abstract

Introduction

Conclusions

References

Tables

Figures



Back

Close

Full Screen / Esc

Printer-friendly Version

Interactive Discussion



Evaluation of CALIOP 532 nm AOD over opaque water clouds

Z. Liu et al.

Title Page

Abstract

Introduction

Conclusions

References

Tables

Figures



Back

Close

Full Screen / Esc

Printer-friendly Version

Interactive Discussion



(Platt, 1973). On the other hand, H is defined as the ratio of the integrated attenuated backscatter from single scattering only ($\gamma'_{WC, SS}$) to the total integrated attenuated backscatter, which includes contributions from multiple scattering ($\gamma'_{WC, MS}$). This ratio is functionally related to the layer integrated depolarization ratio δ_i as described by Eq. (4). $\gamma'_{WC, MS} = \int_{base}^{top} B'(r)dr$ is the layer-integrated attenuated backscatter calculated from opaque water clouds measured by CALIOP (Vaughan et al., 2010), and thus includes not only multiple-scattering effects but also additional attenuation from any overlying cloud or aerosol layers (Hu et al., 2007). The layer-integrated attenuated single-scattering backscatter for a cloud with no aerosol (NA) located above can be calculated from theory using Platt's equation:

$$\gamma'_{WC, SS, NA} = \int_{base}^{top} \beta'_{SS}(r)dr = \frac{1 - \exp(-2\tau)}{2S_{WC}}; \quad (6)$$

$$\approx \frac{1}{2S_{WC}}, \text{ for opaque water clouds } (\tau \gtrsim 3),$$

The last expression holds for water clouds with optical depths greater than about 3. S_{WC} is the water cloud lidar ratio and τ is the cloud optical depth. From Mie calculations based on in-situ measurements of water cloud size distributions (Hu et al., 2006; also see Fig. 2), S_{WC} is found to be relatively invariant for a variety of water clouds measured in situ, having a mean value of 18.9 sr and a standard deviation of 0.25 sr over ocean and 0.47 sr over land. The presence of a semi-transparent aerosol layer above an OWC will reduce $\gamma'_{WC, SS, NA}(r)$ by an amount equal to the two-way transmittance, $\exp(-2\tau_{aerosol})$, of the aerosol layer; i.e., $\gamma'_{WC, SS} = \exp(-2\tau_{aerosol})\gamma'_{WC, SS, NA}$,

where τ_{aerosol} is the optical depth of overlying aerosol layer. Therefore,

$$\tau_{\text{aerosol}} = -\frac{1}{2} \ln \left(\frac{Y'_{\text{WC, SS}}}{Y'_{\text{WC, SS, NA}}} \right). \quad (7a)$$

$$\tau_{\text{aerosol}} = -\frac{1}{2} \ln \left(\frac{HY'_{\text{WC, MS}}}{\frac{1}{2S_{\text{WC}}}} \right) = -\frac{1}{2} \ln \left(2S_{\text{WC}} Y'_{\text{WC, MS}} \left(\frac{1 - \delta_1}{1 + \delta_1} \right)^2 \right) \quad (7b)$$

5 The layer-integrated depolarization ratio within the cloud layer, δ_1 , is calculated from the perpendicular and parallel components of attenuated backscatter measured at 532 nm, β'_{\perp} and β'_{\parallel} ,

$$\delta_1 = \frac{\int_{\text{base}}^{\text{top}} \beta'_{\perp}(r) dr}{\int_{\text{base}}^{\text{top}} \beta'_{\parallel}(r) dr}. \quad (8)$$

10 The AOD determined using the OWC technique can be used as a constraint to retrieve backscatter and extinction profiles and lidar ratio of the overlying aerosol layer. For the cases selected and analyzed in this paper, the underlying clouds are opaque boundary layer clouds with cloud-tops lower than 2 km. Given the relatively small footprint of the CALIOP lidar (100 m), for single-shot retrievals, it is not necessary that the clouds be
 15 overcast on any significant horizontal scale, and the retrieval appears to work well even in broken stratocumulus. A closer examination shows that the temperatures at the top of these opaque clouds typically range from 8 to 25 °C, confirming that these clouds are water.

20 Retrievals from measurements made by passive satellite sensors such as MODIS (Zhang et al., 2011) produce effective radii for water clouds that are generally larger than those obtained from in-situ measurements (Miles et al., 2000). To represent these larger droplet sizes we have extended the previously reported Mie calculations to cloud particle sizes larger than 15 μm . The results are presented in Fig. 2 (solid green

Evaluation of CALIOP
532 nm AOD over
opaque water clouds

Z. Liu et al.

Title Page	
Abstract	Introduction
Conclusions	References
Tables	Figures
◀	▶
◀	▶
Back	Close
Full Screen / Esc	
Printer-friendly Version	
Interactive Discussion	



Evaluation of CALIOP 532 nm AOD over opaque water clouds

Z. Liu et al.

Title Page

Abstract

Introduction

Conclusions

References

Tables

Figures



Back

Close

Full Screen / Esc

Printer-friendly Version

Interactive Discussion



segments in Fig. 5a show a smoke aerosol layer (brown) and an opaque water cloud layer (blue) as detected by the standard CALIOP L2 layer detection algorithm, which is applied to the 532 nm data. However, in the 1064 nm profile shown in Fig. 5b, the base of the smoke layer is seen to extend down to the top of the water cloud. Below about 2.5 km, the 532 nm signal levels of this smoke fall below the detection threshold, and the lower part of the smoke layer is not successfully detected by the standard data processing. 1064 nm signal penetrates further into the smoke layer because the extinction of smoke aerosols is typically 2–3 times smaller at 1064 nm than at 532 nm. The L2 retrieval, however, is only applied to the smoke layer as detected in the 532 nm profile, between ~ 4.5 km and ~ 2.5 km. The averaged aerosol extinction profile from the L2 profile products (dark green) is shown in Fig. 5c.

The OWC constrained retrieval is started at a fixed altitude of 8 km and continues downward to an altitude ~ 0.2 km above the apparent cloud top determined by the L2 processing. The OWC constrained retrieval is performed iteratively, using a set of trial values of lidar ratio. A lidar ratio solution is determined as the value that produces the best match between the AOD retrieved from the attenuated backscatter above the water cloud and the OWC AOD. An extinction profile retrieved using the OWC AOD as a constraint is also presented in Fig. 5c (light green). The OWC-constrained retrieval successfully captures the lower part of the smoke layer that is missed in the L2 processing. Above the smoke layer (~ 4.2 km) the retrieved extinction varies largely due to noise and at a level comparable to the calibration error. After the aerosol extinction is retrieved, particulate polarization ratio (PDR), another aerosol intrinsic property, can be retrieved from the two measured polarization components of backscattered signals at 532 nm using

$$\delta_a(r) = \frac{\beta'_\perp(r) \exp\left(2 \int_{\text{top}}^r \alpha(r) dr\right) - \beta_m(r) \frac{\delta_m}{1+\delta_m}}{\beta'_\parallel(r) \exp\left(2 \int_{\text{top}}^r \alpha(r) dr\right) - \beta_m(r) \frac{1}{1+\delta_m}} \quad (9)$$

where δ_m is the molecular depolarization ratio, with a value of ~ 0.0036 for the spectral bandwidth of the CALIOP receiver (Powell et al., 2009).

3.5 Full column retrieval

The CALIOP feature detection algorithm sometimes cannot successfully detect weakly scattering parts of an aerosol layer or lower parts of highly attenuating aerosol layers, as discussed earlier (also see Figs. 4 and 5). This causes the retrieved AOD to be biased low. To help evaluate the impact of potential failures in detecting full extent of aerosol layers, we also performed full column (FC) retrievals, where the retrieval is initiated at a fixed altitude of 8 km and proceeds downward using a fixed lidar ratio. We use a set of fixed lidar ratios incremented by 5 sr (i.e., 40, 45, etc.) plus the modeled values used in the CALIOP L2 retrievals for different aerosol types. The FC retrieval differs from the CALIOP standard L2 retrieval in that the L2 extinction retrieval is only applied between the top and base of the aerosol layers detected by the SIBYL layer detection algorithm, whereas in the FC retrieval aerosol is assumed to be present throughout the full vertical column extending 8 km down to 0.2 km above the L2-identified top of the underlying OWC. The FC retrieval is terminated above the underlying OWC to avoid possible contamination of cloud edges in the aerosol retrieval. The starting altitude of 8 km was chosen to ensure that the aerosol backscatter coefficients in the upper portion of the retrieval region would lie well below the SIBYL detection threshold, and thus the retrieved AOD would account for all significant aerosol loading in the column. For example, consider the smoke layer around 6.61° S in Fig. 4. Because of the large attenuation at 532 nm (Fig. 5a), the attenuated backscatter coefficients in the lower part of the layer fall below the SIBYL detection threshold, and thus SIBYL detects the base of this layer at ~ 3 km (Fig. 5c). However, as seen in Fig. 5b, the true aerosol layer base appears to extend to the top of the underlying cloud at ~ 1.5 km. For this example, the L2 retrieval would only apply to the upper part of this layer between ~ 5 km and ~ 3 km and hence miss the lower part of this layer between ~ 3 km and ~ 1.5 km and therefore underestimate AOD of the layer (e.g., see Kim et al., 2013). Because the

Evaluation of CALIOP 532 nm AOD over opaque water clouds

Z. Liu et al.

Title Page

Abstract

Introduction

Conclusions

References

Tables

Figures



Back

Close

Full Screen / Esc

Printer-friendly Version

Interactive Discussion



cated above the clouds and those without (based on the VFM and with $|\text{ASR}| < 0.05$). Imposing a criterion of $|\text{ASR}| < 0.05$ ensures that the AOD above the clouds is less than ~ 0.02 , even for strongly absorbing aerosols such as smoke. The subset of OWCs with no overlying aerosols in a $2^\circ \times 3^\circ$ (lat \times lon) grid box was used to calculate a reference

$\gamma'_{\text{WC, SS, NA}}$ which was used in Eq. (6) to retrieve AOD from the subset with overlying aerosol.

4.1 Geographical distributions from OWC retrievals

Because accurate knowledge of $\gamma'_{\text{WC, SS, NA}}$ is so important in the derivation of AOD using the OWC technique, in this subsection we examine the spatial variability of $\gamma'_{\text{WC, SS, NA}}$ and its potential impact on the retrieved AODs. To obtain more insight we look into the geographical distributions of dust and smoke optical properties retrieved using the OWC technique. Figures 6 and 7 present $2^\circ \times 3^\circ$ maps of (a) the number of samples acquired, (b) mean AOD_{OWC} , (c) mean S_a and (d) particulate depolarization ratio (PDR) of aerosol layers using the OWC constrained retrieval technique, respectively, for the dust and smoke transport regions. AOD_{OWC} was calculated using Eq. (6a) with a location-dependent $\gamma'_{\text{WC, SS, NA}}$. Panels (e) through (h) in Figs. 6 and 7 show the same quantities for the data screened using $\text{ASR} > 0.3$ for the dust region and $\text{ASR} > 0.2$ for the smoke regions. The ASR threshold for the smoke region is smaller than for the dust region because for the same extinction the backscatter at 532 nm is smaller for smoke than dust due to the difference in the lidar ratios. Panels (i) through (k) in each figure are the corresponding properties retrieved using a constant value of $\gamma'_{\text{WC, SS, NA}}$ which was averaged over the entire red box for each selected region, and panels (d) through (f) are the differences between these retrieved properties using a location dependent $\gamma'_{\text{WC, SS, NA}}$ (as in panels (i) through (k)) and a constant $\gamma'_{\text{WC, SS, NA}}$ (as in panels (f) through (h)).

Most OWCs are observed just offshore over the northeastern Atlantic and southeastern Atlantic, in the trade wind regions. As expected, AOD_{OWC} is the largest in the

Title Page

Abstract

Introduction

Conclusions

References

Tables

Figures



Back

Close

Full Screen / Esc

Printer-friendly Version

Interactive Discussion



coastal regions near the sources in North and South Africa and decreases gradually as dust or smoke is transported farther from the sources.

The S_a retrieval is sensitive to errors and biases in the AOD_{OWC} and to the noise in the above-cloud backscatter signals. This is especially noticeable when the overlying aerosol layers are optically thin, as will be discussed further in the following subsections. Partly due to this, we see large variations in the retrieved S_a at the edges of the dust transport pathway (Fig. 6c) where AOD_{OWC} is small (Fig. 6b). We also see that the retrieved S_a values are larger outside of the typical dust transport pathway, where the occurrence of dust is less frequent. The PDR, retrieved using Eq. (8) and shown in Fig. 6d, generally has smaller values north of $\sim 30^\circ$ N and south of $\sim 10^\circ$ N, which suggests that considerable amounts of other aerosol types are present outside of the dust transport pathway. North of $\sim 30^\circ$ N the westerly wind (Fig. 1) can carry anthropogenic aerosols having large S_a values from North America to the northwest coast of Africa. South of $\sim 10^\circ$ N, the southeasterly trade wind can bring biomass burning aerosol from central Africa to the tropical North Atlantic (Fig. 1). At 532 nm, biomass burning aerosols (smoke) generally have S_a values larger than dust, as seen by comparing Fig. 7c and g to Fig. 6c and g. The retrieved S_a and PDR for dust are distributed more uniformly when weakly scattering aerosol layers are screened out using $ASR > 0.3$. This is as generally expected and provides confidence to our analysis results. Since a sizeable fraction of North Africa is covered by deserts, desert dust is a dominant aerosol type in this region all year long. During summer, the transport of dust over the Atlantic is usually confined to the free troposphere by two inversions and hence the dust size distribution can remain largely unchanged (Maring et al., 2003). More uniform distributions of S_a and PDR are expected where dust is dominant. Large values (> 60 sr) are, however, still seen south of 10° N, where the transported biomass burning aerosol is relatively dense and dominant.

When a constant $V'_{WC, SS, NA}$ is used, as in the previous work of Chand et al. (2009) and Sakaeda et al. (2011), a larger geographic trend is seen both in S_a (Fig. 6j) and PDR (Fig. 6k) retrieved for dust. A more significant trend is also seen in the retrieved

Evaluation of CALIOP 532 nm AOD over opaque water clouds

Z. Liu et al.

Title Page

Abstract

Introduction

Conclusions

References

Tables

Figures



Back

Close

Full Screen / Esc

Printer-friendly Version

Interactive Discussion



Evaluation of CALIOP 532 nm AOD over opaque water clouds

Z. Liu et al.

Title Page

Abstract

Introduction

Conclusions

References

Tables

Figures



Back

Close

Full Screen / Esc

Printer-friendly Version

Interactive Discussion



S_a for smoke (Fig. 7j). S_a is an intrinsic property of aerosols and is not expected to vary significantly for aerosols generated by the same mechanisms and from the same source regions. The large geographical trend in the retrieved S_a when using a constant $\gamma'_{WC, SS, NA}$ does not appear to be realistic and is correlated with the $\gamma'_{WC, SS, NA}$ distribution in Fig. 3, indicating that the trend in the aerosol retrievals is actually an artifact introduced by the use of a constant $\gamma'_{WC, SS, NA}$. The use of a constant $\gamma'_{WC, SS, NA}$ can overestimate smoke AOD by ~ 0.1 near the source and S_a by ~ 10 sr in the northern part of the selected smoke region while underestimating these properties in the south-western part of the region. This highlights the necessity of using a location-dependent $\gamma'_{WC, SS, NA}$. More discussion on the retrieved aerosol optical properties using a location-dependent $\gamma'_{WC, SS, NA}$ will be provided in the following subsections.

4.2 Dust intrinsic optical properties

One-dimensional (1-D) and two-dimensional (2-D) histograms of the retrieved S_a and PDR using a location-dependent $\gamma'_{WC, SS, NA}$ within the red box over the dust transport region are presented in Fig. 8a through d. The distributions of the retrieved S_a and PDR (Fig. 8c and d) are somewhat asymmetric. The mean value of the dust lidar ratio distribution is 50.5 sr, with a median of 45.5 sr, a mode of 44.0 sr, and a standard deviation of 26.4 sr, while for the PDR distribution the mean is 0.222, the median is 0.277, the mode is 0.280, and the standard deviation is 4.24. When weakly scattering layers are screened out using $ASR > 0.3$, the S_a and PDR distributions become more symmetric. The mean, median, mode and standard deviation of the screened S_a data are, respectively, 45.1, 44.4, 43.3 and 8.8 sr, and, respectively, 0.281, 0.281, 0.283 and 0.044 for the screened PDR data. For either the screened or the unscreened data, the modeled S_a value (40 sr) used to produce CALIOP V3 data is $\sim 10\%$ smaller than the OWC retrieved value (Fig. 8c).

As mentioned earlier S_a is an intrinsic optical property of aerosols that depends on the particle composition, size, and shape, but is independent of particle concentration or loading. The dust S_a values reported in this work fall well within the range of the

**Evaluation of CALIOP
532 nm AOD over
opaque water clouds**

Z. Liu et al.

Title Page

Abstract

Introduction

Conclusions

References

Tables

Figures



Back

Close

Full Screen / Esc

Printer-friendly Version

Interactive Discussion



natural variability of dust lidar ratios previously reported in the scientific literature. An earlier case study based on CALIOP measurements (Liu et al., 2008) tracked a dust event that occurred on 17 August 2006 in North Africa and was subsequently transported across the Atlantic Ocean over the course of several days. The retrieved S_a at 532 nm for this event was 41 ± 3 , 41 ± 4 , 41 ± 6 sr, respectively, at locations near the source, over the eastern and central Atlantic Ocean. The dust was moderately dense with its AOD at 532 nm decreasing from 0.6–1.2 near the source to 0.29 far from the source. The NASA Langley Research Center (LaRC) airborne high-spectral-resolution lidar (HSRL) measured a lidar ratio of 45.8 ± 0.8 sr and AOD of 0.08–0.09 for the dust transported into the Gulf of Mexico 10 days later. Another study (Liu et al., 2011) using multiple years of the CALIOP measurements derived a S_a distribution for opaque dust layers (AOD $\gtrsim 2$) over North Africa with a mean value of 38.5 ± 9.2 sr. It was shown that multiple scattering in these opaque dust layers can decrease the effective lidar ratio by 10% or more relative to the semi-transparent layers analyzed here with the OWC technique.

Shipborne Raman lidar measurements in May 2013 tracked the Saharan air layer across the tropical Atlantic (Kanitz et al., 2014). A 532 nm S_a of 45 sr was measured for aged dust that was ~ 4500 km away from the North Africa, and 50 sr for dust ~ 800 km off the coast of the North Africa. The layers observed ~ 800 km off the coast were not pure dust, but instead were dust mixed with smoke which generally has high S_a values. Over dust source regions in Morocco, S_a was observed in a range of 38–50 sr by an airborne HSRL for pure dust over Morocco during the SAMUM 2006 campaign (Esselborn et al., 2009). Meantime, a range of $53\text{--}55 \pm 7$ sr was observed for selected dust events by ground-based Raman lidars operated at the airport of Ouarzazate in Morocco (Tesche et al., 2009). Back trajectory analyses show that the observed variability in lidar ratio is primarily attributable to differences in source regions. The large deviation of S_a retrieved in this study (Fig. 8a and c) may partly reflect the dependence of the dust optical properties on the sources. Computations based on in-situ measurements (Omar et al., 2010) and AERONET retrievals (Cattrall et al., 2005; Shuster et al.,

region (Fig. 6g) even after screening out weakly scattering layers. Unlike North Africa, where the landmass is largely desert and desert dust is a dominant aerosol type, in central and southern Africa, the human population density is higher and the surface type is more variable. While smoke is the dominant aerosol type during the austral winter, when biomass burning is active, several other types of anthropogenic aerosols can also be present in non-negligible amounts during this time period.

Smoke from biomass fires is dominated by submicron-sized particles, frequently containing internally mixed black carbon (Reid et al., 2005; Li et al., 2003), and produces low PDR and high S_a at 532 nm (Müller et al., 2007; Omar et al., 2009; Burton et al., 2012;). Smoke S_a and PDRs can vary depending on the type of fire, the combustion source and the age of the smoke. The S_a values retrieved in this study are consistent with the case study presented in Hu et al. (2007) that used the OWC constrained technique to obtain a S_a of 66 ± 6 sr for a smoke layer transported from the southern Africa biomass burning region. Our retrieved values are also consistent with values retrieved during the SAFARI 2000 field campaign in northeastern South Africa. Values of 50–90 sr were retrieved from micro-pulse lidar observations of dense smoke (Campbell et al., 2003) and, in cases where the column AOD was dominated by smoke, values of 70–74 sr were obtained by combining airborne backscatter lidar data with ground-based sunphotometer data (McGill et al., JGR 2003). The PDR values retrieved in the smoke region are typically smaller than 0.1, with mode/median/mean values of 0.041/0.036/0.043 \pm 0.64 for all smoke layers analyzed and 0.041/0.036/0.038 \pm 0.026 for the layers with ASR > 0.2. Irrespective of aerosol type, the PDR calculation can be biased significantly by noise when the aerosol layer is weakly scattering. The standard deviation computed from all the analyzed smoke layers is large (2.28), but is reduced to 0.025 when weakly scattering layers are screened out. The PDR distributions appear to be non-Gaussian with a positive skewness. Internally mixed potassium salts and organic particles are the predominant components in the smoke from the African biomass burning, and the smoke particles undergo hygroscopic growth, reaction and transformation. Although dominated by fine mode particles,

Evaluation of CALIOP 532 nm AOD over opaque water clouds

Z. Liu et al.

[Title Page](#)[Abstract](#)[Introduction](#)[Conclusions](#)[References](#)[Tables](#)[Figures](#)[Back](#)[Close](#)[Full Screen / Esc](#)[Printer-friendly Version](#)[Interactive Discussion](#)

large complex chain-like soot aggregates and aggregates of fine particles have been observed in the smoke from the biomass burning in the southern Africa (Li et al., 2003). Unlike the surrounding fine mode particles, these large nonspherical particles strongly depolarize the incident photons and the depolarization ratio of measured backscatter signals from smoke varies depending on the fraction of nonspherical particles.

4.4 CALIOP L2 AOD evaluation

In this subsection, we attempt to evaluate above-cloud AOD produced by the CALIOP L2 standard retrieval and estimate an error budget based on the analysis of the two selected regions. Figures 10 and 11 present comparisons of the analysis results where the OWC retrieval is considered to be “truth”. For the dust transport region, AOD_{L2} is well correlated with AOD_{OWC} (Fig. 10a). However, the mean value for AOD_{L2} is 0.184 (Fig. 10f), which is 25.8 % smaller than the mean value of AOD_{OWC} (0.248). We examine the factors that may contribute to this discrepancy and attempt to estimate an error budget. In the L2 retrieval, the lidar ratio sometimes needs to be adjusted when the retrieval diverges and becomes unstable (Young and Vaughan, 2009). Such cases rarely occur in the dust region ($\sim 2.5\%$ of the retrievals), and are hereafter excluded to simplify the remaining analysis. The CALIOP aerosol classification (Fig. 10e) is dominated by “dust” (contributing 91.4 % of the total AOD), followed by “polluted dust” (8.5 %), consistent with expectations for the area. Assuming that any aerosol type in this region other than “dust” is a misclassification, rescaling the extinction of all non-“dust” range bins using Eq. (4) decreases the AOD only by 0.005. This accounts for only 10.9 % of the AOD discrepancy. This indicates the CALIOP L2 algorithms have been largely successful in correctly identifying the above-cloud aerosol type as “dust” in this region.

As mentioned earlier, the FC retrieval using a fixed S_a can provide insight into the error due to the failure of the L2 algorithms to detect the full vertical extent of aerosol layers. The mean AOD from the FC retrieval using the modeled S_a value (40 sr) for “dust” ($AOD_{FC, mod}$) is 0.202, which is larger than that for the rescaled L2 AOD ($AOD_{L2, res} = 0.177$) by 0.025, but still smaller than AOD_{OWC} by 0.046. We note

Evaluation of CALIOP 532 nm AOD over opaque water clouds

Z. Liu et al.

Title Page

Abstract

Introduction

Conclusions

References

Tables

Figures



Back

Close

Full Screen / Esc

Printer-friendly Version

Interactive Discussion



that $AOD_{L2, res}$ was derived by scaling all other aerosol types to “dust” using Eq. (4). Therefore, the difference between $AOD_{FC, mod}$ and $AOD_{L2, res}$ is mainly due to the failure to detect the full extent of the aerosol layers (e.g., due to inherent detection limits). The failure to detect those parts of the aerosol layer(s) that lie below the CALIOP detection limit may contribute under half (39.0 %; see Table 1) of the total AOD discrepancy. From Fig. 11d we can see that the difference between $AOD_{L2, res}$ and $AOD_{FC, mod}$ comes mainly from the extinction retrieval at lower altitudes. Below 1 km there seems to be some contamination by cloud edges. Although the L2 algorithms fail to detect the aerosol above about 7 km (Fig. 11d), the aerosol loading here is very small and does not contribute significantly to the column AOD. Small differences between the L2 and FC profiles below 2 km indicate the L2 algorithms are doing a moderately good job of detecting the base of the dust layer. The standard CALIOP modeled S_a for dust (40 sr) is $\sim 10\%$ smaller than the OWC retrieved value (Fig. 6h). Differences in S_a have a non-linear effect on the retrieved AOD, and thus this 10 % disparity in S_a contributes the majority (71.9 %) of the total AOD discrepancy, so that, in the mean, AOD_{L2} underestimates AOD_{OWC} by 18.6 %. Table 1 compares all AOD retrievals for the dust transport region. Table 2 shows the error budget estimated for AOD_{L2} in the dust transport regions along with the error budget in the smoke transport region that will be discussed in the next paragraph.

In the smoke transport region, AOD_{L2} is not as well-correlated with AOD_{OWC} as it is in the dust cases discussed above. As seen in Fig. 11f and Table 3, the L2 smoke AOD is 0.191, which is smaller than the smoke AOD_{OWC} (0.311) by 38.6 %. The following factors contribute to this larger AOD discrepancy. As seen in Fig. 11e, the dominant aerosol type in the region, as classified in the CALIOP L2 product, is “smoke” (83.3 % by AOD), which is expected. The next most common type is “polluted dust” (8.4 %), followed by “marine” (4.5 %) and “polluted continental (3.9 %). “Polluted dust” is possible for this area. However, “marine” aerosols are unlikely to be found above the boundary clouds found in this region, and these classifications are thought to arise from a coding error within the aerosol subtyping module. Rescaling the extinction coefficients of those

Evaluation of CALIOP 532 nm AOD over opaque water clouds

Z. Liu et al.

[Title Page](#)[Abstract](#)[Introduction](#)[Conclusions](#)[References](#)[Tables](#)[Figures](#)[Back](#)[Close](#)[Full Screen / Esc](#)[Printer-friendly Version](#)[Interactive Discussion](#)

aerosols classified as types other than “smoke” increases the mean AOD by 0.031 to 0.222, which corresponds to 25.8 % of the total AOD discrepancy, which in turn reduces the L2 AOD underestimation by 10.0 % and improves the correlation with AOD_{OWC} .

$AOD_{FC, mod}$ for the FC retrieval using a modeled S_a of 70 sr for “smoke” is 0.314, larger than the OWC AOD by only 2.5 %. This implies that a failure to detect the full extent of the aerosol layers lying above the clouds, whether due to inherent detection limits or algorithm deficiencies, is responsible for 76.7 % of the AOD discrepancy. The FC retrievals suggest that the L2 layer detection scheme can detect the upper parts of the smoke layers fairly well, but fails to detect a significant fraction of the aerosol below ~ 3 km (Fig. 11d). Smoke aerosols typically have large absorption at visible wavelengths, which increases detection difficulties as the signal penetrates into the lower part of a layer (also see the example in Figs. 4 and 5). Mis-detection of aerosol layer bases, and to a lesser extent layer tops, thus appears to be the main cause for the AOD differences for the case of smoke above opaque clouds.

The S_a values retrieved using AOD_{OWC} as a constraint have a mode/median/mean value of 69.8/71.8/74.8 \pm 17 sr for the screened smoke data. The modeled S_a value of 70 sr (Omar et al., 2009) thus appears to be appropriate and representative for the transported smoke when compared with the OWC-constrained S_a (Fig. 11f). While the mean values for AOD_{OWC} and $AOD_{FC, mod}$ are identical, AOD_{OWC} appears to be a little bit larger than $AOD_{FC, mod}$ for smaller AODs and somewhat smaller for larger AODs (Fig. 11c and f).

4.5 Further comments about Dust Lidar Ratio

To help evaluate CALIOP AOD retrievals, comparison studies have been performed using AERONET measurements (e.g., Amiridis et al., 2013; Schuster et al., 2012) and ground-based Raman lidar measurements (e.g., Tesche et al., 2013). These comparison studies have provided many details useful for a better understanding of the CALIOP AOD retrieval uncertainties. In general, these studies show that the CALIOP version 3 retrievals typically underestimate dust AODs, and are in general agreement with the

results presented in this work. Amiridis et al. (2013) and Tesche et al. (2013) have suggested a lidar ratio of 56–58 sr for the CALIOP dust retrieval based on the ratio of AERONET/ground-based lidar AOD and CALIOP AOD, assuming errors in lidar ratio and AOD are proportional. However, as shown in Winker et al. (2009) and Young et al. (2013), the dependence of the AOD error on the lidar ratio error is nonlinear. The following relationship between the error in AOD and error in S_a is given in Winker et al. (2009),

$$\Delta\tau = \frac{(e^{2\tau'} - 1) \Delta S_a}{2 S_a} = \frac{(e^{2(\tau+\Delta\tau)} - 1) (S'_a - S_a)}{2 S_a}, \quad (10)$$

where $\tau' = \tau + \Delta\tau$ is the retrieved AOD and τ is the true AOD, S_a is the aerosol lidar ratio and S'_a is the lidar ratio used in the retrieval. For small optical depths, the relative error in optical depth is roughly proportional to the relative error in lidar ratio, $\Delta\tau\tau = \Delta S_a/S_a$. As the optical depth increases, the relative error in optical depth increases faster than that in lidar ratio. Figure 12 presents 2-D distributions of FC-retrieved AODs using $S_a = 40, 45, 50, 55$ and 60 sr vs. OWC-retrieved AODs for the same dataset for the dust transport region (JJA 2007–2012), along with the corresponding extinction profiles. The blue lines in panels (a)–(e) indicate the relation expected for a linear scaling, with a slope of $(FC S_a)/(OWC S_a)$. The broken red lines represent the AOD, $\tau' = \tau + \Delta\tau$, numerically calculated using Eq. (10). An iteration of ~ 10 is required in the calculation to solve $\Delta\tau$ which appears on both sides of Eq. (10). It is seen from Fig. 12 that, the FC-OWC AOD distribution generally falls on the linear scaling line for the case of $S_a = 45$ sr which is very close to the retrieved value (44.4 sr) or the cases for smaller AOD values. Significant deviation of the FC-OWC AOD distribution from the linear scaling line starts to occur in the $S_a = 50$ sr case, for example, when OWC AOD ~ 0.4 . Such a nonlinear behavior becomes more significant and the retrieval becomes unstable more frequently as S_a increases.

Nonlinear behavior is also seen in the extinction profiles (Fig. 12f). The effect of a larger lidar ratio on the retrieved extinction profile increases more and more as the

**Evaluation of CALIOP
532 nm AOD over
opaque water clouds**

Z. Liu et al.

Title Page	
Abstract	Introduction
Conclusions	References
Tables	Figures
◀	▶
◀	▶
Back	Close
Full Screen / Esc	
Printer-friendly Version	
Interactive Discussion	



retrieval proceeds from top to bottom. In the FC retrievals, the correction for attenuation during the lidar signal inversion is terminated when the retrieved AOD is unreasonably large (e.g., > 5) to prevent the retrieval blowing up. For this reason, the FC extinction using $S_a = 60$ sr is smaller than that using $S_a = 55$ sr below ~ 0.7 km.

Figure 13 shows the mean AOD_{FC} retrieved using different S_a values as a function of S_a . The corresponding data are listed in Table 4. It is clear that the AOD retrieval is not linearly dependent on S_a . For the FC retrieval using $S_a = 50$ sr, for example, although S_a is increased by 25 % compared with the retrieval using the CALIOP modeled value of $S_a = 40$ sr, the retrieved mean AOD is increased by 66 %, ~ 2.6 times the S_a increase. Therefore, for a more accurate estimate of S_a from the AOD ratio, the nonlinear dependence of AOD on S_a must be taken into account. We note that the S_a and AOD retrieved in this study are effective quantities which have not been corrected for potential effects of multiple scattering. To derive conventional values, consistent with airborne HSRL or AERONET measurements, S_a and AOD should be corrected (i.e., divided by) the appropriate multiple scattering factor, η . Simulations show that the multiple scattering factor is generally around 0.9–0.95 for moderately dense dust layers (Liu et al., 2011) and can decrease to 0.8–0.85 for very dense cases (extinction coefficient $\gtrsim 2$ km⁻¹), although the appropriate value of η depends on the geometric thickness of the dust layer (Winker, 2003).

From the analysis above, increasing the V3 dust lidar ratio (40 sr) by a factor of 1.4–1.45 (i.e., to 56–58 sr) would likely generate unrealistically large AOD estimates for even moderately dense layer (i.e., as in Fig. 12e and f), at least for the region analyzed in this paper. However, increasing the V3 dust lidar ratio from 40 sr to 45 sr would, on average, increase the AOD by a factor of about 1.26.

5 Summary

Validating all aspects of the CALIOP data products is an ongoing task for the CALIPSO team. In this paper, we evaluated CALIOP retrievals of aerosols above water clouds, for

Title Page

Abstract

Introduction

Conclusions

References

Tables

Figures



Back

Close

Full Screen / Esc

Printer-friendly Version

Interactive Discussion



with $ASR > 0.3$. The corresponding PDR for smoke is 0.036 ± 0.64 for all smoke layers and 0.036 ± 0.026 for smoke layers having $ASR > 0.2$

When comparing the AOD reported in the CALIPSO Level 2 data products to the OWC-retrieved AOD, the retrieved L2 AOD underestimates the measured OWC AOD by 25.8% in the dust transport region (0.184 for L2 vs. 0.248 for OWC). This AOD underestimate increases to 38.6% in the smoke transport region (0.191 for L2 vs. 0.311 for OWC). When partitioning the errors into a comprehensive error budget we find that the CALIOP aerosol subtyping algorithm performs well in the dust region during nighttime: 90.9% of all layers are classified as “dust” and 8.87% of layers are classified “polluted dust”. Misclassification of aerosol subtype is thus responsible for 10.9% (an overestimate) of the total discrepancy between the L2 and OWC retrievals, which compensates somewhat the underestimate effect from other error sources. Failure to detect the full geometric extent of the dust layers is responsible for an additional -39.0% (negative sign indicating an underestimate) of the error budget. The largest contributor to the L2 underestimate of dust AOD is due to the difference between the CALIOP modeled dust lidar ratio and the OWC measured values. While the L2-modeled and OWC-measured lidar ratio values are different by only $\sim 10\%$, the nonlinear relationship between S_a and AOD results in lidar ratio differences being the root cause for -71.9% of the L2 AOD underestimation.

The L2 aerosol retrieval generates a more substantial underestimate of AOD in the smoke transport region. However, in the smoke region the differences between the L2-modeled and OWC-measured lidar ratios are negligible, thus make no meaningful contribution to the overall error budget. Possible misclassification of aerosol subtype accounts for -25.8% and the layer detection failure contributes the most (-76.7%) to the underestimation of the L2 smoke AOD.

Evaluation of CALIOP
532 nm AOD over
opaque water clouds

Z. Liu et al.

Title Page	
Abstract	Introduction
Conclusions	References
Tables	Figures
◀	▶
◀	▶
Back	Close
Full Screen / Esc	
Printer-friendly Version	
Interactive Discussion	



References

- Amiridis, V., Wandinger, U., Marinou, E., Giannakaki, E., Tsekeri, A., Basart, S., Kazadzis, S., Gkikas, A., Taylor, M., Baldasano, J., and Ansmann, A.: Optimizing CALIPSO Saharan dust retrievals, *Atmos. Chem. Phys.*, 13, 12089–12106, doi:10.5194/acp-13-12089-2013, 2013.
- 5 Burton, S. P., Ferrare, R. A., Hostetler, C. A., Hair, J. W., Rogers, R. R., Obland, M. D., Butler, C. F., Cook, A. L., Harper, D. B., and Froyd, K. D.: Aerosol classification using airborne High Spectral Resolution Lidar measurements – methodology and examples, *Atmos. Meas. Tech.*, 5, 73–98, doi:10.5194/amt-5-73-2012, 2012.
- 10 Cattrall, C., Reagan, J., Thome, K., and Dubovik, O.: Variability of aerosol and spectral lidar and backscatter and extinction ratios of key aerosol types derived from selected Aerosol Robotic Network locations, *J. Geophys. Res.*, 110, D10S11, doi:10.1029/2004JD005124, 2005.
- Chand, D., Wood, R., Anderson, T. L., Satheesh, S. K., and Charlson, R. J.: Satellite-derived direct radiative effect of aerosols dependent on cloud cover, *Nat. Geosci.*, 2, 181–184, 2009.
- 15 Climate Change 2013: The Physical Science Basis. Contribution of Working Group I to the Fifth Assessment Report of the Intergovernmental Panel on Climate Change, edited by: Stocker, T. F., Qin, D., Plattner, G.-K., Tignor, M., Allen, S. K., Boschung, J., Nauels, A., Xia, Y., Bex, V., and Midgley, P. M., Cambridge University Press, Cambridge, UK and New York, NY, USA, 1535 pp., 2013.
- 20 Cook, J. and Highwood, E. J.: Climate response to tropospheric absorbing aerosol in an intermediate general-circulation model, *Q. J. Roy. Meteor. Soc.*, 130, 175–191, 2004.
- Cooke, W., Koffi, B., and Cregoire, J. M.: Seasonality of vegetation fires in African from remote sensing data and application to a global chemistry model, *J. Geophys. Res.*, 101, 21051–21065, 1996.
- Elterman, L.: Aerosol measurements in the troposphere and stratosphere, *Appl. Optics*, 5, 1769–1776, 1966.
- 25 Esselborn, M., Wirth, M., Fix, A., Weinzierl, B., Rasp, K., Tesche, M., and Petzold, A.: Spatial distribution and optical properties of Saharan dust observed by airborne high spectral resolution lidar during SAMUM 2006, *Tellus B*, 61, 131–143, doi:10.1111/j.1600-0889.2008.00394.x, 2009.
- 30 Fernald, F. G.: Analysis of atmospheric lidar observations: some comments, *Appl. Optics*, 23, 652–653, 1984.

Evaluation of CALIOP 532 nm AOD over opaque water clouds

Z. Liu et al.

Title Page

Abstract

Introduction

Conclusions

References

Tables

Figures



Back

Close

Full Screen / Esc

Printer-friendly Version

Interactive Discussion



Evaluation of CALIOP 532 nm AOD over opaque water clouds

Z. Liu et al.

[Title Page](#)
[Abstract](#)
[Introduction](#)
[Conclusions](#)
[References](#)
[Tables](#)
[Figures](#)

[Back](#)
[Close](#)
[Full Screen / Esc](#)
[Printer-friendly Version](#)
[Interactive Discussion](#)


Freudenthaler, V., Esselborn, M., Wiegner, M., Althausen, D., Wirth, M., Fix, A., Ehret, G., Knippertz, P., Toledano, C., Gasteiger, J., Garhammer, M., and Seefeldne, M.: Depolarization ratio profiling at several wavelengths in pure Saharan dust during SAMUM 2006, *Tellus B*, 61, 165–79, 2009.

5 Hansen, J., Sato, M., and Ruedy, R.: Radiative forcing and climate response, *J. Geophys. Res.*, 102, 6831–6864, 1997.

Haywood, J. M., Pelon, J., Formenti, P., Bharmal, N., Brooks, M., Capes, G., Chazette, P., Chou, C., Christopher, S., Coe, H., Cuesta, J., Derimian, Y., Desboeufs, K., Greed, G., Harrison, M., Heese, B., Highwood, E. J., Johnson, B., Mallet, M., Marticorena, B., Marsham, J., Mil-
10 ton, S., Myhre, G., Osborne, S. R., Parker, D. J., Rajot, J.-L., Schulz, M., Slingo, A., Tanre, D., and Tulet, P.: Overview of the dust and biomass-burning experiment and African monsoon multidisciplinary analysis special observing period-0, *J. Geophys. Res.*, 113, D00C17, doi:10.1029/2008JD010077, 2008.

Hu, Y.: Depolarization ratio–effective lidar ratio relation: theoretical basis for space lidar cloud phase discrimination, *Geophys. Res. Lett.*, 34, L11812, doi:10.1029/2007GL029584, 2007.

Hu, Y., Vaughan, M., Winker, D., Liu, Z., Noel, V., Bissonnette, L., Roy, G., McGill, M., and Trepte, C.: A simple multiple scattering-depolarization relation of water clouds and its potential applications, in: *Proceedings of 23rd International Laser Radar Conference*, Nara, Japan, 24–28 July, 19–22, 2006.

20 Hu, Y., Vaughan, M., Liu, Z., Powell, K., and Rodier, S.: Retrieving optical depths and lidar ratios for transparent layers above opaque water clouds from CALIPSO lidar measurements, *IEEE T. Geosci. Remote*, 4, 523–526, 2007.

Hu, Y., Winker, D., Vaughan, M., Lin, B., Omar, A., Trepte, C., Flittner, D., Yang, P., Sun, W., Liu, Z., Wang, Z., Young, S., Stamnes, K., Huang, J., Kuehn, R., Baum B., and Holz R.: CALIPSO/CALIOP cloud phase discrimination algorithm, *J. Atmos. Ocean. Tech.*, 26, 2293–
25 309, 2009.

Huneus, N., Schulz, M., Balkanski, Y., Griesfeller, J., Prospero, J., Kinne, S., Bauer, S., Boucher, O., Chin, M., Dentener, F., Diehl, T., Easter, R., Fillmore, D., Ghan, S., Ginoux, P., Grini, A., Horowitz, L., Koch, D., Krol, M. C., Landing, W., Liu, X., Mahowald, N., Miller, R., Morcrette, J.-J., Myhre, G., Penner, J., Perlwitz, J., Stier, P., Takemura, T., and Zender, C. S.:
30 Global dust model intercomparison in AeroCom phase I, *Atmos. Chem. Phys.*, 11, 7781–7816, doi:10.5194/acp-11-7781-2011, 2011.

Evaluation of CALIOP 532 nm AOD over opaque water clouds

Z. Liu et al.

[Title Page](#)
[Abstract](#)
[Introduction](#)
[Conclusions](#)
[References](#)
[Tables](#)
[Figures](#)

[Back](#)
[Close](#)
[Full Screen / Esc](#)
[Printer-friendly Version](#)
[Interactive Discussion](#)


- Kanitz, T., Engelmann, R., Heinold, B., Baars, H., Skupin, A., and Ansmann, A.: Tracking the Saharan Air Layer with shipborne lidar across the tropical Atlantic, *Geophys. Res. Lett.*, 41, 1044–1050, doi:10.1002/2013GL058780, 2014.
- Karyampudi, V. M., Palm, S. P., Reagen, J. A., Fang, H., Grant, W. B., Hoff, R. M., Moulin, C., Pierce, H. F., Torres, O., Browell, E. V., and Melfi, S. H.: Validation of the Saharan Dust Plume Conceptual Model using lidar, meteosat, and ECMWF data, *B. Am. Meteorol. Soc.*, 80, 1045–1075, 1999.
- Keil, A. and Haywood, J. M.: Solar radiative forcing by biomass burning aerosol particles during SAFARI 2000: a case study based on measured aerosol and cloud properties, *J. Geophys. Res.*, 108, 8467, doi:10.1029/2002JD002315, 2003.
- Kim, M. H., Kim, S. W., Yoon, S. C., and Omar, A. H.: Comparison of aerosol optical depth between CALIOP and MODIS-Aqua for CALIOP aerosol subtypes over the ocean, *J. Geophys. Res.-Atmos.*, 118, 13241–13252, 2013.
- Kinne, S., Schulz, M., Textor, C., Guibert, S., Balkanski, Y., Bauer, S. E., Berntsen, T., Berglen, T. F., Boucher, O., Chin, M., Collins, W., Dentener, F., Diehl, T., Easter, R., Feichter, J., Fillmore, D., Ghan, S., Ginoux, P., Gong, S., Grini, A., Hendricks, J., Herzog, M., Horowitz, L., Isaksen, I., Iversen, T., Kirkevåg, A., Kloster, S., Koch, D., Kristjansson, J. E., Krol, M., Lauer, A., Lamarque, J. F., Lesins, G., Liu, X., Lohmann, U., Montanaro, V., Myhre, G., Penner, J., Pitari, G., Reddy, S., Seland, O., Stier, P., Takemura, T., and Tie, X.: An AeroCom initial assessment – optical properties in aerosol component modules of global models, *Atmos. Chem. Phys.*, 6, 1815–1834, doi:10.5194/acp-6-1815-2006, 2006.
- Kittaka, C., Winker, D. M., Vaughan, M. A., Omar, A., and Remer, L. A.: Intercomparison of column aerosol optical depths from CALIPSO and MODIS-Aqua, *Atmos. Meas. Tech.*, 4, 131–141, doi:10.5194/amt-4-131-2011, 2011.
- Koffi, B., Schulz, M., Breon, F.-M., Griesfeller, J., Griesfeller, J., Winker, D., Balkanski, Y., Bauer, S., Berntsen, T., Chin, M., Collins, W. D., Dentener, F., Diehl, T., Easter, R., Ghan, S., Ginoux, P., Gong, S., Horowitz, L. W., Iversen, T., Kirkevåg, A., Koch, D., Krol, M., Myhre, G., Stier, P., and Takemura, T.: Application of the CALIOP layer product to evaluate the vertical distribution of aerosols estimated by global models: AeroCom phase I results, *J. Geophys. Res.*, 117, D10201, doi:10.1029/2011JD016858, 2012.
- Levine, J. S., Coffer III, W. R., Cahoon Jr., D. R., and Winstead, E. L.: A driver for global change, *Environ. Sci. Technol.*, 29, 120–125, 1995.

**Evaluation of CALIOP
532 nm AOD over
opaque water clouds**

Z. Liu et al.

Title Page

Abstract

Introduction

Conclusions

References

Tables

Figures



Back

Close

Full Screen / Esc

Printer-friendly Version

Interactive Discussion



- Li, J., Posfai, M., Hobbs, P. V., and Buseck, P. R.: Individual aerosol particles from biomass burning in southern Africa: 2. compositions and aging of inorganic particles, *J. Geophys. Res.*, 108, 8484, doi:10.1029/2002JD002310, 2003.
- Liu, D., Wang, Z., Liu, Z., M. Winker, D., and Trepte, C.: A height resolved global view of dust aerosols from the first year CALIPSO lidar measurements, *J. Geophys. Res.*, 113, D16214, doi:10.1029/2007JD009776, 2008.
- Liu, Z., Omar, A., Vaughan, M., Hair, J., Kittaka, C., Hu, Y., Powell, K., Trepte, C., Winker, D., Hostetler, C., Ferrare, R., and Pierce, R.: CALIPSO lidar observations of the optical properties of Saharan dust: a case study of long-range transport, *J. Geophys. Res.*, 113, D07207, doi:10.1029/2007JD008878, 2008.
- Liu, Z., Vaughan, M. A., Winker, D. M., Kittaka, C., Getzewich, B. J., Kuehn, R. E., Omar, A., Powell, K., Trepte, C. R., and Hostetler, C. A.: The CALIPSO lidar cloud and aerosol discrimination: version 2 algorithm and initial assessment of performance, *J. Atmos. Ocean. Tech.*, 26, 1198–1213, doi:10.1175/2009JTECHA1229.1, 2009.
- Liu, Z., Winker, D., Omar, A., Vaughan, M., Trepte, C., Hu, Y., Powell, K., Sun, W., and Lin, B.: Effective lidar ratios of dense dust layers over North Africa derived from the CALIOP measurements, *J. Quant. Spectrosc. Ra.*, 112, 204–213, doi:10.1016/j.jqsrt.2010.05.006, 2011.
- Lopes, F. J. S., Landulfo, E., and Vaughan, M. A.: Evaluating CALIPSO's 532 nm lidar ratio selection algorithm using AERONET sun photometers in Brazil, *Atmos. Meas. Tech.*, 6, 3281–3299, doi:10.5194/amt-6-3281-2013, 2013.
- Maring, H., Savioe, D. L., Izaguirre, M. A., Custals, L., and Reid, J. S.: Mineral dust aerosol size distribution change during atmospheric transport, *J. Geophys. Res.*, 108, 8592, doi:10.1029/2002JD002536, 2003.
- McGill, M. J., Hlavka, D. L., Hart, W. D., Welton, E. J., and Campbell, J. R.: Airborne lidar measurements of aerosol optical properties during SAFARI-2000, *J. Geophys. Res.*, 108, 8493, doi:10.1029/2002JD002370, 2003.
- Miles, N. J., Verlinde, J., and Clothiaux E. E.: Cloud droplet size distributions in low-level stratiform clouds, *J. Atmos. Sci.*, 57, 295–311, 2000.
- Muller, D., Ansmann, A., Mattis, I., Tesche, M., Wandinger, U., Althausen, D., and Pisani, G.: Aerosol-type-dependent lidar ratios observed with Raman lidar, *J. Geophys. Res.-Atmos.*, 112, D16202, doi:10.1029/2006jd008292, 2007.
- O'Connor, E. J., Illingworth, A. J., and Hogan, R. J.: A technique for autocalibration of cloud lidar, *J. Atmos. Ocean. Tech.*, 21, 777–786, 2004.

**Evaluation of CALIOP
532 nm AOD over
opaque water clouds**

Z. Liu et al.

[Title Page](#)[Abstract](#)[Introduction](#)[Conclusions](#)[References](#)[Tables](#)[Figures](#)[Back](#)[Close](#)[Full Screen / Esc](#)[Printer-friendly Version](#)[Interactive Discussion](#)

- Omar, A., Winker, D., Kittaka, C., Vaughan, M., Liu, Z., Hu, Y., Trepte, C., Rogers, R., Ferrare, R., Kuehn, R., and Hostetler, C.: The CALIPSO automated aerosol classification and lidar ratio selection algorithm, *J. Atmos. Ocean. Tech.*, 26, 1994–2014, doi:10.1175/2009JTECHA1231.1, 2009.
- 5 Omar, A., Liu, Z., Vaughan, M., Thornhill, K. L., Kittaka, C., Ismail, S., Hu, Y., Chen, G., Winker, D., Trepte, C., Winstead, E. L., and Anderson, E. B.: Extinction-to-backscatter ratios of Saharan dust layers derived from in situ measurements and CALIPSO overflights during NAMMA, *J. Geophys. Res.*, 115, D24217, doi:10.1029/2010JD014223, 2010.
- Omar, A. H., Winker, D. M., Tackett, J., Giles, D., Kar, J., Liu, Z., Vaughan, M., Powell, K., and
10 Trepte, C.: CALIOP and AERONET aerosol optical depth comparisons: one size fits none, *J. Geophys. Res.*, 118, 4748–4766, doi:10.1002/jgrd.50330, 2013.
- Pinnick, R. G., Jennings, S. G., Chylek, P., Ham, C., and Grandy Jr., W. T.: Backscatter and extinction in water clouds, *J. Geophys. Res.*, 88, 6787–6796, 1983.
- Platt, C. M. R.: Lidar and radiometric observations of cirrus clouds, *J. Atmos. Sci.*, 30, 1191–
15 1204, 1973.
- Podgorny, I. A. and Ramanathan, V.: A modeling study of the direct effect of aerosols over the tropical Indian Ocean, *J. Geophys. Res.*, 106, 24097–24105, 2001.
- Powell, K. A., Hostetler, C. A., Liu, Z., Vaughan, M. A., Kuehn, R. E., Hunt, W. H., Lee, K., Trepte, C. R., Rogers, R. R., Young, S. A., and Winker, D. M.: CALIPSO lidar calibration algorithms: Part I – Nighttime 532 nm parallel channel and 532 nm perpendicular channel, *J. Atmos. Ocean. Tech.*, 26, 2015–2033, 2009.
- 20 Redemann, J., Vaughan, M. A., Zhang, Q., Shinozuka, Y., Russell, P. B., Livingston, J. M., Kacenelenbogen, M., and Remer, L. A.: The comparison of MODIS-Aqua (C5) and CALIOP (V2 & V3) aerosol optical depth, *Atmos. Chem. Phys.*, 12, 3025–3043, doi:10.5194/acp-12-3025-2012, 2012.
- 25 Reid, J. S., Koppmann, R., Eck, T. F., and Eleuterio, D. P.: A review of biomass burning emissions part II: intensive physical properties of biomass burning particles, *Atmos. Chem. Phys.*, 5, 799–825, doi:10.5194/acp-5-799-2005, 2005.
- Sassen, K. and Cho, B. S.: Subvisual thin cirrus lidar dataset for satellite verification and climatological research, *J. Appl. Meteorol.*, 31, 1275–1285, 1992.
- 30 Schulz, M., Textor, C., Kinne, S., Balkanski, Y., Bauer, S., Berntsen, T., Berglen, T., Boucher, O., Dentener, F., Guibert, S., Isaksen, I. S. A., Iversen, T., Koch, D., Kirkevåg, A., Liu, X., Montanaro, V., Myhre, G., Penner, J. E., Pitari, G., Reddy, S., Seland, Ø., Stier, P., and Takemura, T.:

Evaluation of CALIOP 532 nm AOD over opaque water clouds

Z. Liu et al.

[Title Page](#)
[Abstract](#)
[Introduction](#)
[Conclusions](#)
[References](#)
[Tables](#)
[Figures](#)

[Back](#)
[Close](#)
[Full Screen / Esc](#)
[Printer-friendly Version](#)
[Interactive Discussion](#)


Radiative forcing by aerosols as derived from the AeroCom present-day and pre-industrial simulations, *Atmos. Chem. Phys.*, 6, 5225–5246, doi:10.5194/acp-6-5225-2006, 2006.

Schuster, G. L., Vaughan, M., MacDonnell, D., Su, W., Winker, D., Dubovik, O., Lapyonok, T., and Trepte, C.: Comparison of CALIPSO aerosol optical depth retrievals to AERONET measurements, and a climatology for the lidar ratio of dust, *Atmos. Chem. Phys.*, 12, 7431–7452, doi:10.5194/acp-12-7431-2012, 2012.

Tesche, M., Ansmann, A., Müller, D., Althausen, D., Mattis, I., Heese, B., Freudenthaler, V., Wiegner, M., Esselborn, M., Pisani, G., and Knippertz, P.: Vertical profiling of Saharan dust with Raman lidars and airborne HSRL in southern Morocco during SAMUM, *Tellus B*, 61, 144–164, doi:10.1111/j.1600-0889.2008.00390.x, 2009.

Tesche, M., Wandinger, U., Ansmann, A., Althausen, D., Müller, D., and Omar, A. H.: Ground-based validation of CALIPSO observations of dust and smoke in the Cape Verde region, *J. Geophys. Res.*, 118, 1–14, doi:10.1002/jgrd.50248, 2013.

Textor, C., Schulz, M., Guibert, S., Kinne, S., Balkanski, Y., Bauer, S., Bernsten, T., Berglen, T., Boucher, O., Chin, M., Dentener, F., Diehl, T., Easter, R., Feichter, H., Fillmore, D., Ghan, S., Ginoux, P., Gong, S., Grini, A., Hendricks, J., Horowitz, L., Huang, P., Isaksen, I., Iversen, I., Kloster, S., Koch, D., Kirkevåg, A., Kristjansson, J. E., Krol, M., Lauer, A., Lamarque, J. F., Liu, X., Montanaro, V., Myhre, G., Penner, J., Pitari, G., Reddy, S., Seland, Ø., Stier, P., Takemura, T., and Tie, X.: Analysis and quantification of the diversities of aerosol life cycles within AeroCom, *Atmos. Chem. Phys.*, 6, 1777–1813, doi:10.5194/acp-6-1777-2006, 2006.

Vaughan, M. A., Powell, K. A., Kuehn, R. E., Young, S. A., Winker, D. M., Hostetler, C. A., Hunt, W. H., Liu, Z., McGill, M. J., and Getzewich, B. J.: Fully automated detection of cloud and aerosol layers in the CALIPSO lidar measurements, *J. Atmos. Ocean. Tech.*, 26, 2034–2050, 2009.

Vernier, J. P., Pommereau, J. P., Garnier, A., Pelon, J., Larsen, N., Nielsen, J., Christensen, T., Cairo, F., Thomason, L. W., Leblanc, T., and McDermid, I. S.: The tropical stratospheric aerosol layer from CALIPSO lidar observations, *J. Geophys. Res.*, 114, D00H10, doi:10.1029/2009JD011946, 2009.

Washington, R. W., Todd, M. C., Middleton, N., and Goudie, A. S.: Dust-storm source areas determined by the total ozone monitoring spectrometer and surface observations, *Ann. Assoc. Am. Geogr.*, 93, 297–313, 2003.

Winker, D.: Accounting for multiple scattering in retrievals from space lidar, in: 12th International Workshop on Lidar Multiple Scattering Experiments, edited by: Werner, C., Oppel, U. G.,

**Evaluation of CALIOP
532 nm AOD over
opaque water clouds**

Z. Liu et al.

[Title Page](#)[Abstract](#)[Introduction](#)[Conclusions](#)[References](#)[Tables](#)[Figures](#)[Back](#)[Close](#)[Full Screen / Esc](#)[Printer-friendly Version](#)[Interactive Discussion](#)

and Rother, T., International Society for Optical Engineering, SPIE Proceedings, Vol. 5059, Oberpfaffenhofen, Germany, 128–139, 2003.

Winker, D. M., Vaughan, M. A., Omar, A. H., Hu, Y., Powell, K. A., Liu, Z., Hunt, W. H., and Young, S. A.: Overview of the CALIPSO mission and CALIOP data processing algorithms, J. Atmos. Ocean. Tech., 26, 2310–2323, 2009.

Winker, D. M., Tackett, J. L., Getzewich, B. J., Liu, Z., Vaughan, M. A., and Rogers, R. R.: The global 3-D distribution of tropospheric aerosols as characterized by CALIOP, Atmos. Chem. Phys., 13, 3345–3361, doi:10.5194/acp-13-3345-2013, 2013.

Young, S. A.: Lidar analysis of lidar backscatter profiles in optically thin clouds, Appl. Optics, 34, 7019–7031, 1995.

Young, S. A. and Vaughan, M. A.: The retrieval of profiles of particulate extinction from Cloud Aerosol Lidar Infrared Pathfinder Satellite Observations (CALIPSO) data: algorithm description, J. Atmos. Ocean. Tech., 26, 1105–1119, 2009.

Young, S. A., Vaughan, M. A., Kuehn, R. E., and Winker, D. M.: The retrieval of profiles of particulate extinction from Cloud-Aerosol Lidar Infrared Pathfinder Satellite Observations (CALIPSO) data: uncertainty and error sensitivity analyses, J. Atmos. Ocean. Tech., 30, 395–428, doi:10.1175/JTECH-D-12-00046.1, 2013.

Yu, H., Chin, M., Winker, D. M., Omar, A. H., Liu, Z., Kittaka, C., and Diehl, T.: Global view of aerosol vertical distributions from CALIPSO lidar measurements and GO-CART simulations: regional and seasonal variations, J. Geophys. Res., 115, D00H30, doi:10.1029/2009JD013364, 2010.

Yu, H., Zhang, Y., Chin, M., Liu, Z., Omar, A., Remer, L. A., Yang, Y., Yuan, T., and Zhang, J.: An integrated analysis of aerosol above clouds from A-Train multi-sensor measurements, Remote Sens. Environ., 121, 125–131, 2012.

Zhang, Z. and Platnick, S.: An assessment of differences between cloud effective particle radius retrievals for marine water clouds from three MODIS spectral bands, J. Geophys. Res., 116, D20215, doi:10.1029/2011JD016216, 2011.

Evaluation of CALIOP 532 nm AOD over opaque water clouds

Z. Liu et al.

Table 1. AOD retrievals for dust transport region over North Atlantic.

Different Retrievals	Mean AOD	AOD – AOD _{OWC} (fractional difference)
OWC constrained, AOD _{OWC}	0.248	
L2 standard, AOD _{L2}	0.184	–0.064 (–25.8%)
L2 rescaled, AOD _{L2, res}	0.177	–0.071 (–28.6%)
Full column ($S_a = 40$), AOD _{FC, mod}	0.202	–0.046 (–18.5%)
Full column ($S_a = 45$), AOD _{FC, 45}	0.258	0.010 (4.0%)
CALIOP subtype	Mean L2 AOD	L2 AOD Fraction
Marine	0.000	0.0%
Dust	0.168	91.4%
Polluted dust	0.016	8.5%
Polluted continental	0.000	0.0%
Clean continental	0.000	0.1%
Smoke	0.000	0.2%

[Title Page](#)[Abstract](#)[Introduction](#)[Conclusions](#)[References](#)[Tables](#)[Figures](#)[Back](#)[Close](#)[Full Screen / Esc](#)[Printer-friendly Version](#)[Interactive Discussion](#)

Evaluation of CALIOP 532 nm AOD over opaque water clouds

Z. Liu et al.

Table 3. AOD retrievals for smoke transport region over South Atlantic.

Different Retrievals	Mean AOD	AOD – AOD _{OWC} (fractional difference)
OWC constrained, AOD _{OWC}	0.311	
L2 standard, AOD _{L2}	0.191	–0.120 (–38.6%)
L2 rescaled, AOD _{L2, res}	0.222	–0.089 (–28.6%)
Full column ($S_a = 70$), AOD _{FC, mod}	0.314	0.003 (1.0%)
Full column ($S_a = 75$), AOD _{FC, 75}	0.384	0.073 (23.5%)
CALIOP Subtype	Mean L2 AOD	L2 AOD Fraction
Marine	0.008	4.5%
Dust	0.001	0.2%
Polluted dust	0.016	8.4%
Polluted continental	0.007	3.9%
Clean continental	0.000	0.0%
Smoke	0.159	83.3%

[Title Page](#)[Abstract](#)[Introduction](#)[Conclusions](#)[References](#)[Tables](#)[Figures](#)[Back](#)[Close](#)[Full Screen / Esc](#)[Printer-friendly Version](#)[Interactive Discussion](#)

Evaluation of CALIOP 532 nm AOD over opaque water clouds

Z. Liu et al.

[Title Page](#)[Abstract](#)[Introduction](#)[Conclusions](#)[References](#)[Tables](#)[Figures](#)[Back](#)[Close](#)[Full Screen / Esc](#)[Printer-friendly Version](#)[Interactive Discussion](#)**Table 4.** Mean AOD_{FC} using different S_a values.

S_a (sr)	40	45	50	55	60
$S_a/S_a = 40$	1.00	1.125	1.25	1.375	1.50
AOD _{FC}	0.200	0.253	0.326	0.423	0.532
AOD _{FC} /AOD _{FC} ($S_a = 40$)	1.00	1.26	1.63	2.11	2.66

**Evaluation of CALIOP
532 nm AOD over
opaque water clouds**

Z. Liu et al.

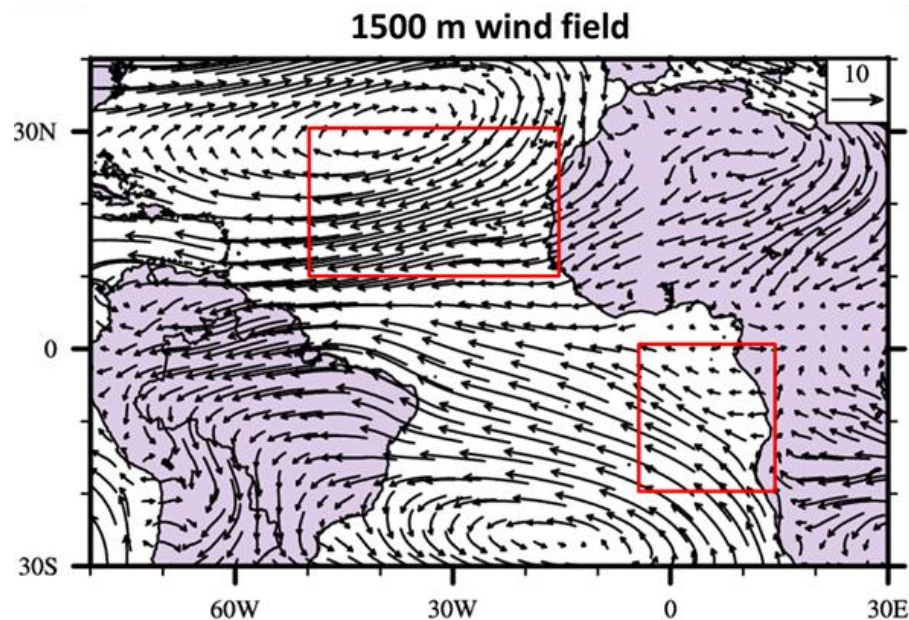


Figure 1. Geographical regions analyzed (red boxes) and wind field (arrows) from ECMWF data for July and August from 2007 to 2012.

[Title Page](#)[Abstract](#)[Introduction](#)[Conclusions](#)[References](#)[Tables](#)[Figures](#)[◀](#)[▶](#)[◀](#)[▶](#)[Back](#)[Close](#)[Full Screen / Esc](#)[Printer-friendly Version](#)[Interactive Discussion](#)

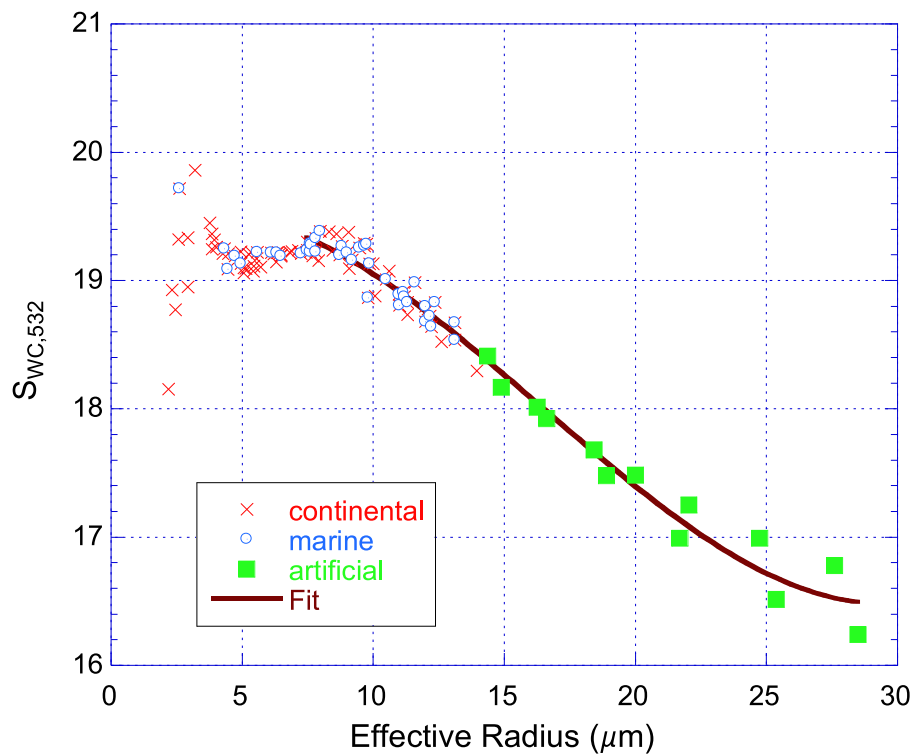


Figure 2. Lidar ratios calculated as function of effective droplet radius for water clouds measured in situ (red crosses and blue diamonds) (Miles et al., 2000) and modeled (green squares) for clouds having larger droplet sizes. The solid curve is a fit.

Evaluation of CALIOP
532 nm AOD over
opaque water clouds

Z. Liu et al.

Title Page	
Abstract	Introduction
Conclusions	References
Tables	Figures
◀	▶
◀	▶
Back	Close
Full Screen / Esc	
Printer-friendly Version	
Interactive Discussion	



Evaluation of CALIOP 532 nm AOD over opaque water clouds

Z. Liu et al.

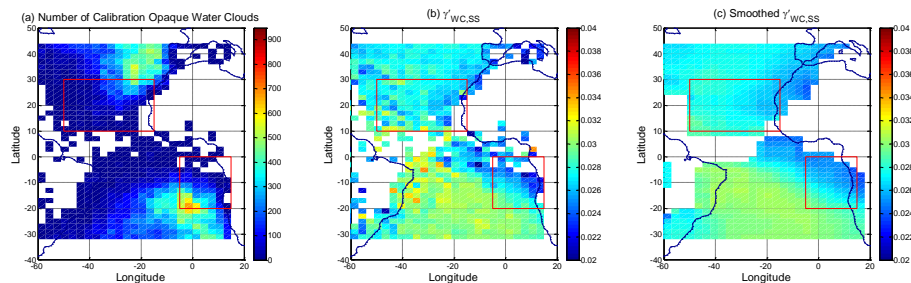


Figure 3. (a) Number of opaque water clouds above which no other cloud or aerosol layer was detected, (b) median integrated attenuated backscatter with correction for multiple scattering $\gamma'_{wc,ss}$ calculated from opaque water clouds in (a), and (c) smoothed $\gamma'_{wc,ss}$ which is used as a reference in each grid box. The grid box size is $2^\circ \times 3^\circ$ (lat \times lon). The smoothing window is 2×2 grid. Data is from all nighttime CALIOP measurements during June–August in the years 2007–2012.

[Title Page](#)
[Abstract](#)
[Introduction](#)
[Conclusions](#)
[References](#)
[Tables](#)
[Figures](#)
[Back](#)
[Close](#)
[Full Screen / Esc](#)
[Printer-friendly Version](#)
[Interactive Discussion](#)


Evaluation of CALIOP
532 nm AOD over
opaque water clouds

Z. Liu et al.

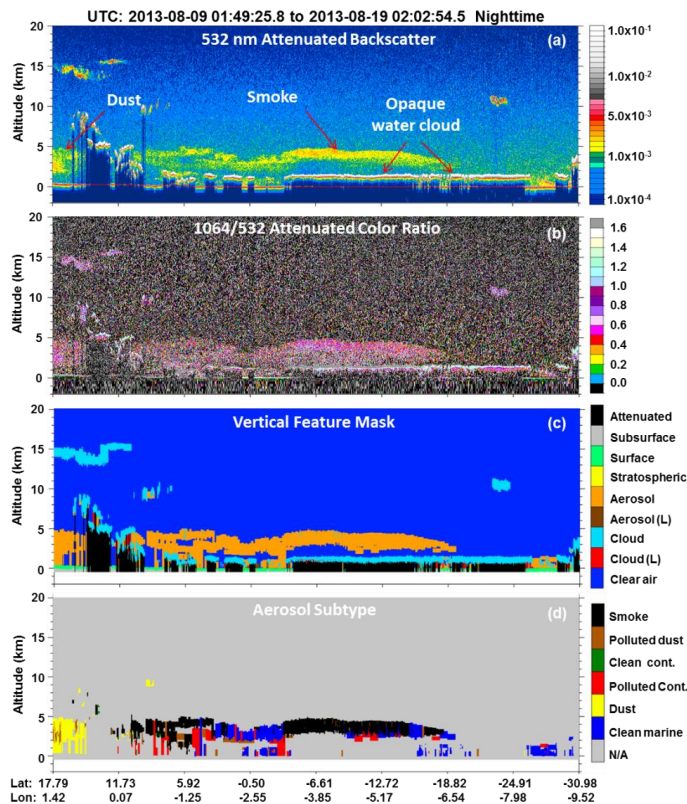


Figure 4. Example of CALIOP measurements of aerosols (smoke and dust) over water clouds made on 9 August 2013. **(a)** 532 nm attenuated backscatter, **(b)** attenuated backscatter color ratio (1064/532), **(c)** vertical feature mask, and **(d)** aerosol subtype.

Title Page

Abstract Introduction

Conclusions References

Tables Figures

◀ ▶

◀ ▶

Back Close

Full Screen / Esc

Printer-friendly Version

Interactive Discussion



Evaluation of CALIOP 532 nm AOD over opaque water clouds

Z. Liu et al.

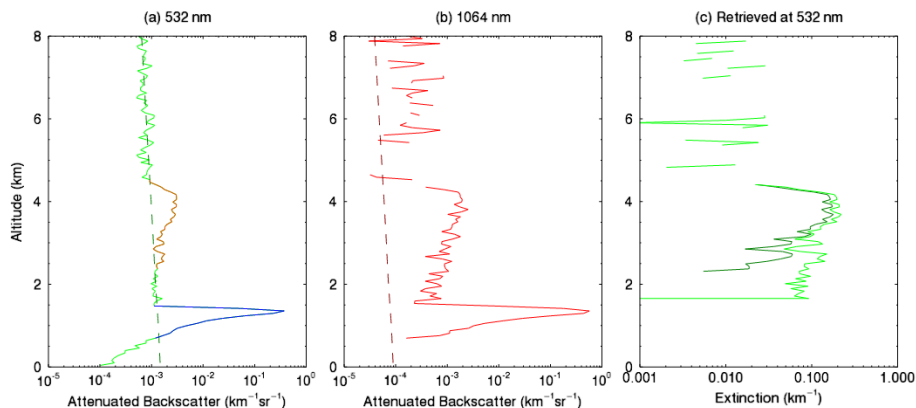


Figure 5. Example of attenuated backscatter profiles corrected for attenuation of molecular scattering and ozone absorption, B' (solid curves) measured by CALIOP at 532 nm **(a)** and 1064 nm **(b)** along with molecular backscatter profiles (broken lines), and aerosol extinction profiles at 532 nm obtained from the standard L2 profile products (dark green) and retrieved in this paper using the OWC constrained technique (light green). Retrieval was applied to each 5 km averaged L1 profiles. All profiles were averaged further for 4 consecutive 5 km profiles around 10° S as shown in Fig. 2. Brown and blue coloring in **(a)** indicate the data segments detected as aerosol and cloud in the standard L2 data processing.

[Title Page](#)
[Abstract](#)
[Introduction](#)
[Conclusions](#)
[References](#)
[Tables](#)
[Figures](#)

[Back](#)
[Close](#)
[Full Screen / Esc](#)
[Printer-friendly Version](#)
[Interactive Discussion](#)


Evaluation of CALIOP 532 nm AOD over opaque water clouds

Z. Liu et al.

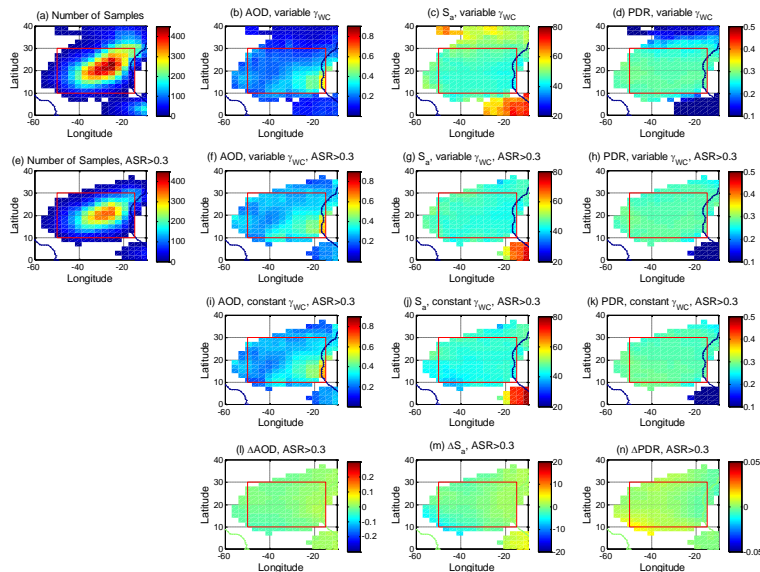


Figure 6. Analysis results over the eastern North Atlantic from CALIOP data acquired during months of June–August in years of 2007–2012. **(a)** Number of samples, **(b)** AOD retrieved using the OWC technique with a location-dependent γ_{WC} for aerosol layers located above the opaque water clouds, and **(c)** S_a and **(d)** particulate depolarization ratio (PDR) retrieved using the OWC-retrieved AOD in **(b)** as a constraint. Shown in the second row of panels **(e–h)** are corresponding maps with data screening of $ASR > 0.3$ for the overlying aerosol layers (i.e., relatively weakly scattering aerosol layers are excluded). The third row of panels **(i–k)** are corresponding maps using a constant $\gamma'_{WC,SS,NA}$. The bottom row of panels **(l–n)** are the difference of the corresponding quantities retrieved using a constant and a geolocation dependent $\gamma'_{WC,SS,NA}$. The size of each grid box is $2^\circ \times 3^\circ$ (lat \times lon). A larger trend depending on geolocation is seen in the intrinsic dust optical properties S_a and PDR retrieved using a constant γ_{WC} **(j)** and **(k)** than using a location-dependent γ_{WC} **(g)** and **(h)**.

Title Page

Abstract

Introduction

Conclusions

References

Tables

Figures

◀

▶

◀

▶

Back

Close

Full Screen / Esc

Printer-friendly Version

Interactive Discussion



Evaluation of CALIOP 532 nm AOD over opaque water clouds

Z. Liu et al.

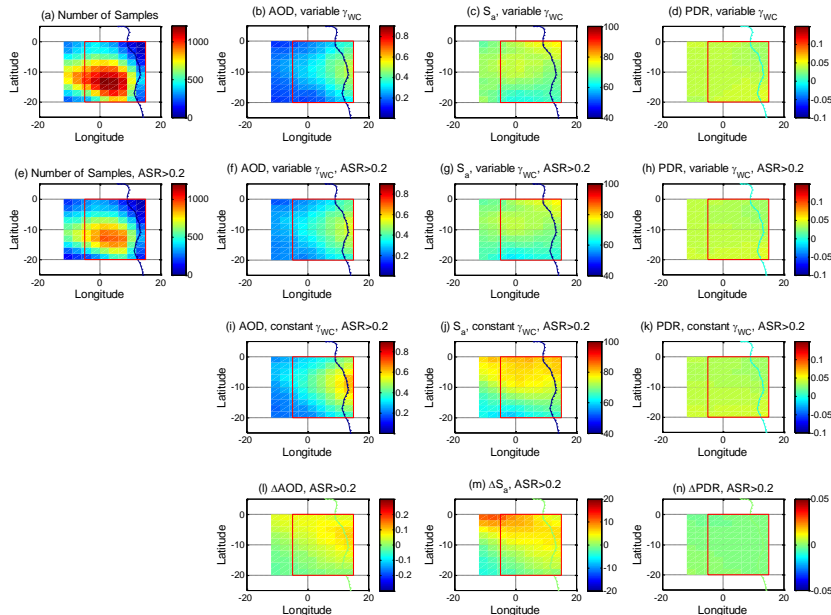


Figure 7. Analysis results over the eastern South Atlantic from CALIOP data acquired during months of July–September in years of 2007–2012. **(a)** Number of samples, **(b)** AOD retrieved using the OWC technique with a location-dependent γ_{WC} for aerosol layers located above the opaque water clouds, and **(c)** S_a and **(d)** particulate depolarization ratio (PDR) retrieved using the OWC-retrieved AOD in **(b)** as a constraint. Shown in the second row of panels **(e–h)** are corresponding maps with data screening of $ASR > 0.2$ for the overlying aerosol layers (i.e., relatively weakly scattering aerosol layers are excluded). The third row of panels **(i–k)** are corresponding maps using a constant $\gamma'_{WC, SS, NA}$. The bottom row of panels **(l–n)** are the difference of the corresponding quantities retrieved using a constant and a location-dependent $\gamma'_{WC, SS, NA}$. The size of each grid box is $2^\circ \times 3^\circ$ (lat \times lon). A significant location-dependent trend is seen in the smoke S_a **(j)** retrieved using a constant γ_{WC} .

Evaluation of CALIOP 532 nm AOD over opaque water clouds

Z. Liu et al.

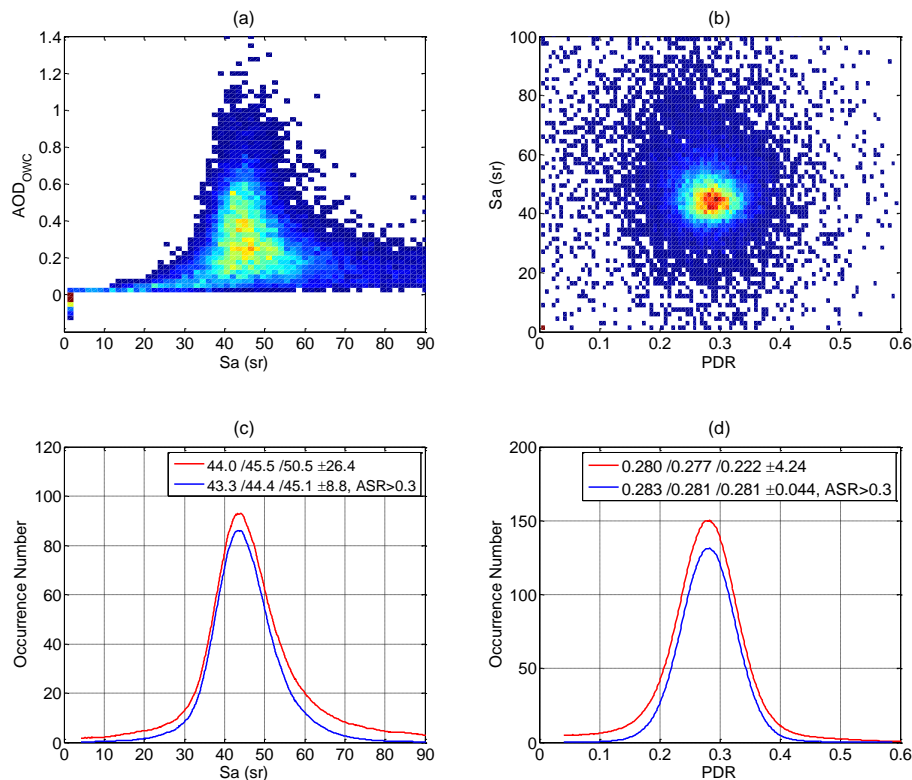


Figure 8. Analysis results for the dust transport region as indicated by the red box in Fig. 6. Two dimensional distributions of **(a)** OWC AOD vs. S_a retrieved using OWC AOD as a constraint, **(b)** S_a vs. PDR; histograms of **(c)** S_a and **(d)** PDR. The S_a distribution in **(a)** has a bin size of 0.1 sr and is smoothed, while the bin size for S_a in **(a)** and **(b)** is 1.5 sr. The PDR distribution in **(c)** has a bin size of 0.001 and is smoothed, while the bin size in **(b)** is 0.006. The red curves in **(c)** and **(d)** include all data and the blue curves are screened data using ASR > 0.3.

Title Page

Abstract

Introduction

Conclusions

References

Tables

Figures

◀

▶

◀

▶

Back

Close

Full Screen / Esc

Printer-friendly Version

Interactive Discussion



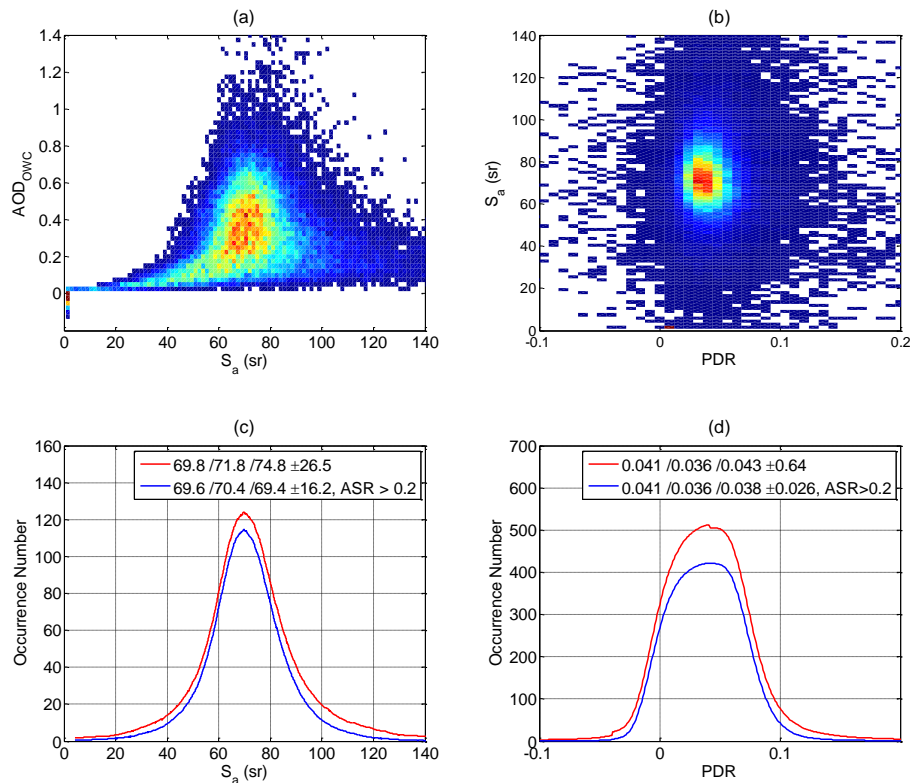


Figure 9. Analysis results for the smoke transport region as indicated by the red box in Fig. 7. Two dimensional distributions of **(a)** AOD_{owc} vs. S_a retrieved using AOD_{owc} as a constraint and **(b)** S_a vs. PDR; histograms of **(c)** S_a and **(d)** PDR. The S_a distribution in **(c)** has a bin size of 0.1 sr and is smoothed, while the bin size for S_a in **(a)** and **(b)** is 1.5 sr. The PDR distribution in **(d)** has a bin size of 0.001 and is smoothed, while the bin size in **(b)** is 0.008. The bin size for AOD in **(a)** is 0.025. The red curves in **(c)** and **(d)** include all data and the blue curves are screened data using ASR > 0.2.

Evaluation of CALIOP 532 nm AOD over opaque water clouds

Z. Liu et al.

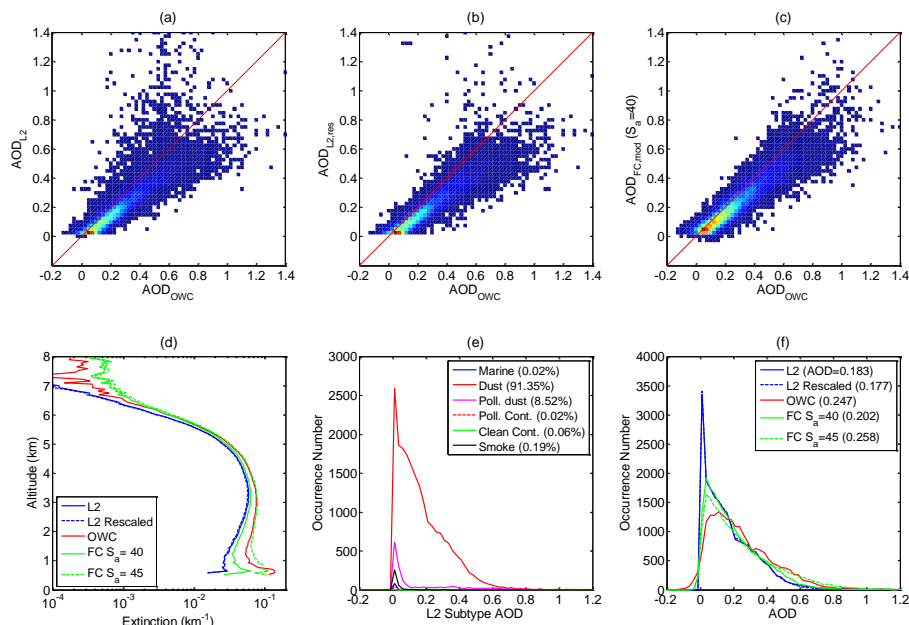


Figure 10. Analysis results for the dust transport region as indicated by the red box in Fig. 6. The top row shows two dimensional distributions of **(a)** AOD_{L2} vs. AOD_{OWC} , **(b)** $AOD_{L2, res}$ vs. AOD_{OWC} , and **(c)** $AOD_{FC, mod}$ vs. AOD_{OWC} for $S_a = 40$ sr. The bottom row shows **(d)** mean extinction profiles and histograms of occurrence number of **(e)** L2 AOD of different aerosol types, and **(f)** AOD retrieved using different retrieval methods. The bin size for AOD is 0.025.

[Title Page](#)
[Abstract](#)
[Introduction](#)
[Conclusions](#)
[References](#)
[Tables](#)
[Figures](#)
[◀](#)
[▶](#)
[◀](#)
[▶](#)
[Back](#)
[Close](#)
[Full Screen / Esc](#)
[Printer-friendly Version](#)
[Interactive Discussion](#)


Evaluation of CALIOP 532 nm AOD over opaque water clouds

Z. Liu et al.

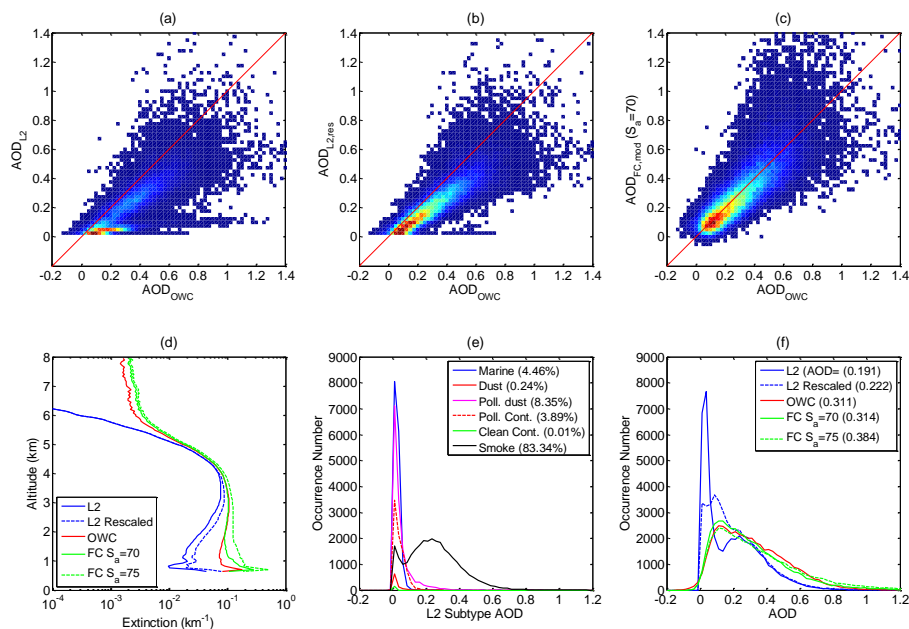


Figure 11. Analysis results for the smoke transport region as indicated by the red box in Fig. 7. The top row shows two dimensional distributions of **(a)** AOD_{L2} vs. AOD_{OWC} , **(b)** $AOD_{L2, res}$ vs. AOD_{OWC} , and **(c)** $AOD_{FC, mod}$ vs. AOD_{OWC} for $S_a = 70$ sr. full column AOD using modeled dust $S_a = 40$ sr vs. AOD_{OWC} . The bottom row shows and **(d)** extinction profiles and histograms of occurrence number of **(e)** L2 AOD of different aerosol types, and **(f)** AOD retrieved using different retrieval methods. The bin size for AOD is 0.025.

[Title Page](#)
[Abstract](#)
[Introduction](#)
[Conclusions](#)
[References](#)
[Tables](#)
[Figures](#)
[⏪](#)
[⏩](#)
[⏴](#)
[⏵](#)
[Back](#)
[Close](#)
[Full Screen / Esc](#)
[Printer-friendly Version](#)
[Interactive Discussion](#)


Evaluation of CALIOP 532 nm AOD over opaque water clouds

Z. Liu et al.

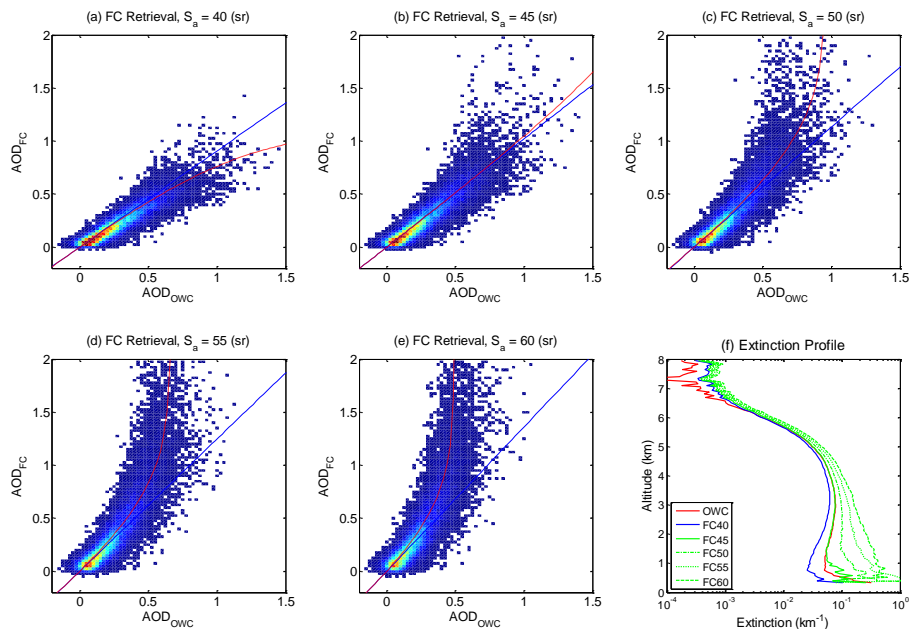


Figure 12. Distributions of FC AOD retrieved from the dust transport region using lidar ratios of **(a)** 40, **(b)** 45, **(c)** 50, **(d)** 55 and **(e)** 60 sr as a function of OWC AOD, and **(f)** corresponding extinction profiles. The blue line in panel **(a–e)** is a line having a slope of FC S_a /OWC S_a . The slope is **(a)** $40/44.4 = 0.91$, **(b)** $45/44.4 = 1.01$, **(c)** $50/44.4 = 1.13$, **(d)** $55/44.4 = 1.24$, and **(e)** $60/44.4 = 1.35$. The red line is AOD estimated using Eq. (10) for a given lidar ratio used in the FC retrieval.

Evaluation of CALIOP
532 nm AOD over
opaque water clouds

Z. Liu et al.

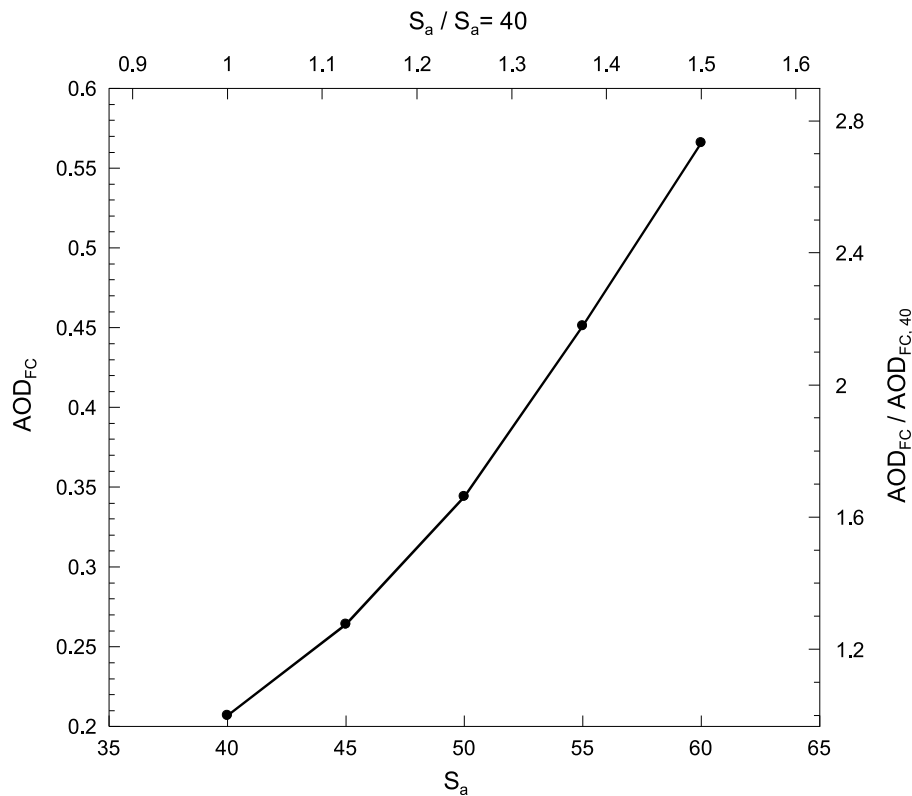


Figure 13. Mean AOD_{FC} as a function of S_a derived from the full column retrievals shown in Fig. 12.

Title Page	
Abstract	Introduction
Conclusions	References
Tables	Figures
◀	▶
◀	▶
Back	Close
Full Screen / Esc	
Printer-friendly Version	
Interactive Discussion	

